Electronic Supplementary Material (ESI) for Journal of Materials Chemistry C.

Supporting Information

Assembly effect on the charge carrier mobility in quaterthiophene-based *n/p*-materials

A. López-Andarias,[a] C. Atienza,[a] J. López-Andarias,[a] W. Matsuda,[b] T. Sakurai,[b] Shu Seki,[b] N. Martín*[a,c]

[a] Departamento de Química Orgánica I, Facultad de Química, Universidad Complutense, E-28040 Madrid, Spain.

[b] Department of Molecular Engineering, Graduate School of Engineering, Kyoto University

[c] IMDEA-Nanociencia, C/ Faraday, 9, Campus de Cantoblanco, E-28049 Madrid, Spain

Table of Contents

1. Materials and methods

Reagents were purchased from Sigma-Aldrich, Acros or Fluka and were used without further purification. All solvents were dried by means of standard protocols with sodium and benzophenone as indicator. Column chromatography was carried out on silica gel 60 (Fluka, 40-63 μm). Reverse phase chromatography was carried out on an Agilent flash chromatography system with pre-packed flash chromatography columns (TELOS, Flash C18 12g). IR spectra were recorded on a Bruker Tensor 27 spectrometer equipped with ATR and reported as wavenumbers in $cm^{-1}$with band intensities indicated as s (strong), m (medium), w (weak), br (broad). ^{1}H and ^{13}C NMR spectra were recorded either on a Bruker Avance-300 or a BrukerAvance AMX-700 and reported as chemical shifts (δ) in ppm relative to tetramethylsilane ($\delta = 0$) at room temperature unless other temperature was indicated. Spin multiplicities are reported as a singlet (s), broad singlet (br s), doublet (d), triplet (t) and quartet (q) with proton-proton coupling constants (*J*) given in Hz, or multiplet (m). Matrix-assisted laser desorption ionization (MALDI) mass spectrometry (MS) was performed on a Bruker Ultraflex spectrometer using ditranol as matrix. Absorption spectra were recorded with a Varian Cary 50 and 5000 spectrophotometer and UV-3600 Shimadzu UV-vis-NIR Spectrophotometer. The anisotropic absorption spectroscopy was carried out with a JASCO V-570 spectrometer with a polarizer. CD measurements were carried out on a JASCO J-815 DC spectrometer. Fluorescence images were recorded on a Leica SP2 confocal microscope (λ_{exc}= 380 nm).

X-ray photoelectron spectroscopy (XPS): the analysis was obtained on a SPECS GmbH (PHOIBOS 150 9 MCD) spectrometer working in the constant analyzer energy mode and a non-monochromatic aluminium X-ray source (1486.61 eV) powered at 200 W and a voltage of 12 eV. For recording both survey and high resolution spectra pass energies of 75 and 25 eV were applied. Survey data were acquired from kinetic energies of 1487 – 400 eV with 0.1 eV of energy step and 100 ms dwell time per point. The high resolution scans were registered around the significant emission lines with 0.1 eV steps and 100 ms dwell time per point. The spectrometer control and data handling were monitorized using SpecsLab Version 2.48 software. Binding energies were calibrated relatively to the C 1s peak at 284.6 eV and the atomic ratios were computed from experimental intensity rations.

Transmission Electron Microscopy (TEM): TEM images were performed in a JEOL JEM 1011 electron microscope operated at 100 kV. Images were directly recorded using a GATAN Erlangshen ES 1000W camera attached to the microscope. In the case of HR-TEM, images were acquired in a JEOL JEM 3000F electron microscope operated at 300 kV.

Scanning Electron Microcopy (SEM): SEM images were acquired on a JEOL JSM 6335F microscope working at 10 kV, by depositing the sample on graphite and metallizing with Au before observation.

2. Synthesis.

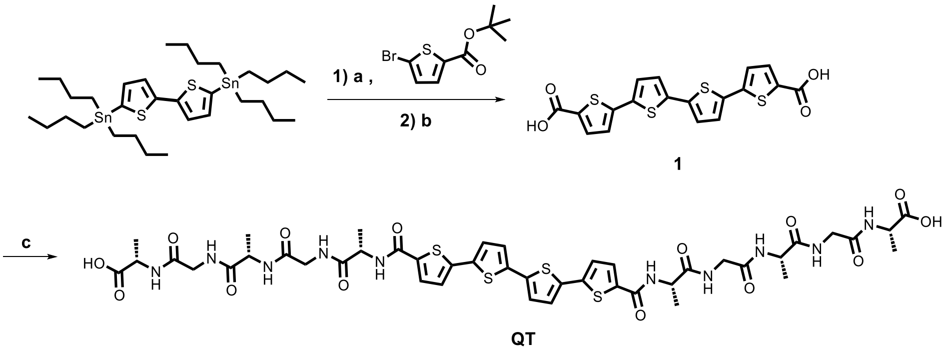

Scheme S1. Synthesis of **QT**. (a) $Pd(PPh_3)_4$, DMF, 80 ºC; (b) CH_2Cl_2/TFA (3:2), rt, 70% (2 steps); (c) i) HATU, TEA, DMF, rt; ii) AGAGA, Na_2CO_3, THF/1,4-Dioxane/H_2O (1:1:1), rt, 84%.

[2,2’;5’,2’’;5’’,2’’’]-quaterthiophene-5,5’’’dicarboxylic acid, 1. The α,α’ oligothiophenedicarboxylic acid precursor was prepared as described in detail elsewhere.[1]

N-[[2,2’;5’,2’’;5’’,2’’’]-quaterthiophene-5,5’’’-biscarbonyl]-L-alanylglycyl-L-alanylglycyl-L-alanine, QT.

To a solution of **1** (20mg, 0.048 mmol) in 2 mL of anhydrous DMF, HATU (40 mg, 0.106 mmol) and TEA (19 μL, 0.134 mmol) were added. This mixture stirred at room temperature under inert atmosphere for 5 minutes. Meanwhile the pentapeptide,L-Alanyl-glycyl-L-alanyl-glycyl-L-alanine trifluoroacetate, was stirred at room temperature in 1.5 mL of a 1:1:1 mixture of 1,4-dioxane, THF and Na_2CO_3 aqueous solution (2 M). The latter solution was added to the activated dicarboxilic acid precursor and the resultant mixture stirred 2 hours at room temperature under Ar flow. The solvent mixture was then removed after reduced pressure and the crude reaction redissolved in water. The solution was injected in a flash purification system to be purified by reverse phase chromatography in a water-methanol gradient (from 0 to 100 % in 20 minutes with a flow rate of 12 mL/min). Pure product was obtained as an orange powder (48 mg, 94%). IR: 3285 (w), 2985 (m), 1624 (s), 1517 (s), 1231 (m); ^1H NMR (DMSO-*d6*, 700 MHz): 8.87 (br s, 2H), 8.44 (br s, 2H), 8.26 (br s, 2H), 8.15 (br s, 2H), 7.49 (br s, 2H), 7.45 (d, J = 5.1 Hz, 2H), 7.38-7.36 (m, 6H), 4.41-4.37 (m, 2H), 4.19-4.15 (m, 2H), 4.83-4.71 (m, 6H), 3.64-3.61 (m, 2H), 3.44-3.41 (m, 2H), 1.35 (d, J = 7.1 Hz, 6H), 1.22 (d, J = 7.1 Hz 6H), 1.18 (d, J = 7.1 Hz 6H)); ^{13}CNMR (DMSO-*d6*, 176 MHz): 173.6, 172.5, 169.0, 167.7, 161.1, 140.2, 139.2, 136.0, 135.7, 130.9, 126.8, 126.2, 125.4, 50.4, 50.1, 48.9, 43.2, 42.7, 19.5, 18.2, 17.7; MS (MALDI) calculated for $C_{44}H_{52}N_{10}NaO_{14}S_4$ ($[M+Na]^+$): 1095.24; found: 1095.2

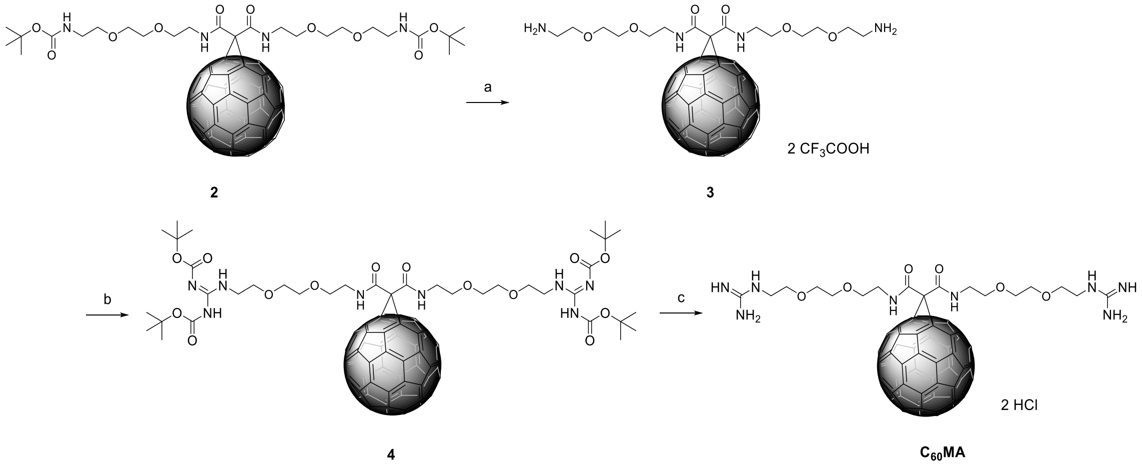

Scheme S2. (a) TFA, $CHCl_3$, rt; (b) 1,3-Bis(*tert*-butoxycarbonyl)-2-methyl-2-thiopseudourea, TEA, $HgCl_2$, DMF, rt; (c) HCl (aq), CH_3OH, rt

Compound 2. To a solution of C_{60} (500 mg, 0.694 mmol) in 250 mL of anhydrous toluene, I_2 (180 mg, 0.694 mmol) and N(1),N(3)-bis-*tert*-Butyl-2-[2-(2-aminoethoxy)ethoxy]ethylcarbamate]malonamide (192 mg, 0.316 mmol)[2] were added. A solution of DBU (150 µL, 0.948 mmol) in 20 mL of toluene was then added dropwise. The mixture was stirred under inert atmosphere overnight. The solvent was removed under reduced pressure and the residue purified in silica gel flash chromatography (eluent: toluene to complete elution of free C_{60}, then CH_2Cl_2 to CH_2Cl_2/CH_3OH, 30:1). Pure product was obtained as a brown powder (226 mg, 25%). IR: 3270 (m), 2923 (m), 1709 (s), 1658 (s), 1274 (m), 1119 (m); ^1H NMR ($CDCl_3$, 500 MHz): 3.78-3.68 (m, 8H), 3.63-3.50 (m, 12H), 3.33 (bs, 4H), 1.45 (s, 18H); ^{13}CNMR ($CDCl_3$, 126 MHz): 155.8, 145.1, 144.7, 144.6, 144.4, 144.3, 143.7, 143.0, 142.9, 142.9, 142.2, 142.1, 140.8, 137.8, 70.3, 70.2, 69.6, 40.4, 29.6, 28.4; HRMS (MALDI) calculated for $C_{85}H_{46}N_4NaO_{10}$ ($[M+Na]^+$): 1305.3112; found: 1305.3074

Compound 3. **2** (110 mg, 0.086 mmol) was dissolved in 5 mL of $CHCl_3$ and 1.5 mL of TFA were added dropwisely. Reaction stirred overnight and the solvent was removed under reduced pressure. The crude product was washed with DCM and pure product was obtained as a dark-brown solid (92 mg, quant.). IR: 2924 (m), 1679 (s), 1563 (m), 1203 (m), 1134 (m); ^{1}H NMR (MeOD-*d4* - $CDCl_3$ 1:2, 500 MHz): 3.93-3.83 (m, 24H); ^{13}CNMR (MeOD-*d4* - $CDCl_3$ 1:2, 126 MHz): 163.4, 146.3, 145.3, 145.0, 144.6, 144.5, 144.4, 144.2, 143.6, 142.9, 142.8, 142.7, 141.9, 140.7, 137.4, 70.1, 69.8, 69.4, 66.2, 40.1, 39.2; HRMS (MALDI) calculated for $C_{75}H_{32}N_4O_6$ ($[M+H]^+$): 1083.2243; found: 1083.2223

Compound 4. To a dispersion of **3** (65 mg, 0.06 mmol) in 7 mL of $CHCl_3$, triethylamine (40 µL, 0.3 mmol) was added. The mixture stirred 5 minutes at r.t and some drops of MeOH were added until complete solution of the starting material. Then 1,3-Bis(*tert*-butoxycarbonyl)-2-methyl-2-thiopseudourea (32 mg, 0.109 mmol). Reaction stirred at 40 ºC for three days. The crude reaction was purified in silica gel flash chromatography with a CH_2Cl_2/CH_3OH, (30:1) mixture as eluent to yield pure product as a brown solid (49 mg, 52%). IR: 3275 (m), 2923 (m), 1722 (s), 1652 (s), 1565 (m); 1362 (m), 1139 (s); ^{1}H NMR ($CDCl_3$, 500 MHz): 11.48 (s, 2H), 8.58 (s, 2H), 7.62 (s, 2H), 3.78-3.69 (m, 8H), 3.63-3.59 (m, 12H), 1.49 (s, 36H); ^{13}CNMR ($CDCl_3$, 126 MHz): 163.7, 162.9, 156.4, 153.2, 146.2, 145.5, 145.4, 145.4, 144.9, 144.9, 144.6, 144.0, 143.3, 142.4, 142.3, 141.1, 138.2, 83.2, 79.4, 70.6, 69.5, 40.8, 40.7, 28.5, 28.3; MS (MALDI) calculated for $C_{97}H_{66}N_8NaO_{14}$ ($[M+Na]^+$): 1589.46; found: 1589.5

C_{60}MA. Chlorhydric acid (0.5 mL, 4.5 mmol) was added to a dispersion of **4** (70 mg, 0.045 mmol) in 2.5 mL of a 1:4 $CHCl_3$ and MeOH mixture. This mixture stirred at r.t. for two days. The solvents mixture was removed under reduced pressure and the crude product washed with DCM. Pure product was obtained as dark-brown solid (46 mg, 88%). IR: 3245 (m), 2920 (m), 1644 (s), 1603 (s), 1538 (m); 1083 (m); ^{1}H NMR (DMSO-d_6, 700 MHz): 9.76 (s, 24H), 7.61 (s, 2H), 7.24 (bs, 6H) 1.59-3.48 (m, 24H); ^{13}CNMR (DMSO-d_6, 176 MHz): 161.4, 157.0, 147.6, 145.6, 144.3, 144.2, 143.8, 143.3, 143.0, 142.2, 142.1, 142.1, 141.6, 141.5, 139.8, 136.6, 74.9, 69.6, 68.7, 68.4; HRMS (MALDI) calculated for $C_{77}H_{34}N_8NaO_6$ ($[M+Na]^+$): 1189.2499; found: 1189.2494

3. NMR spectra

^{1}H-NMR and ^{13}C-NMR of **QT** (DMSO-d_6)

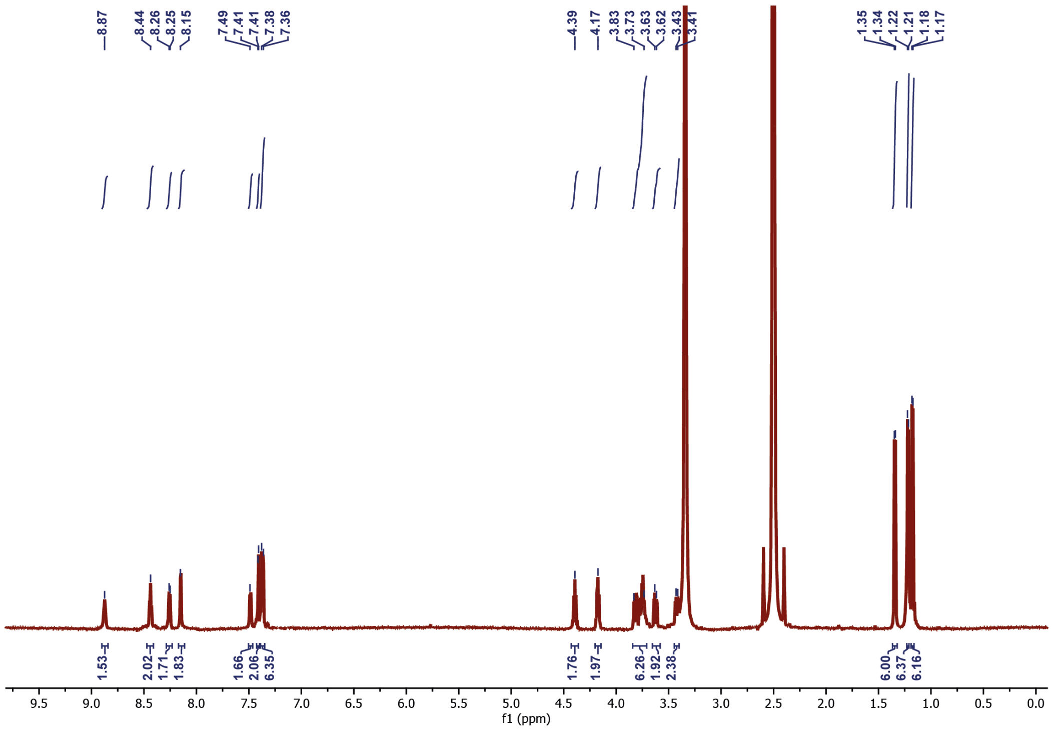

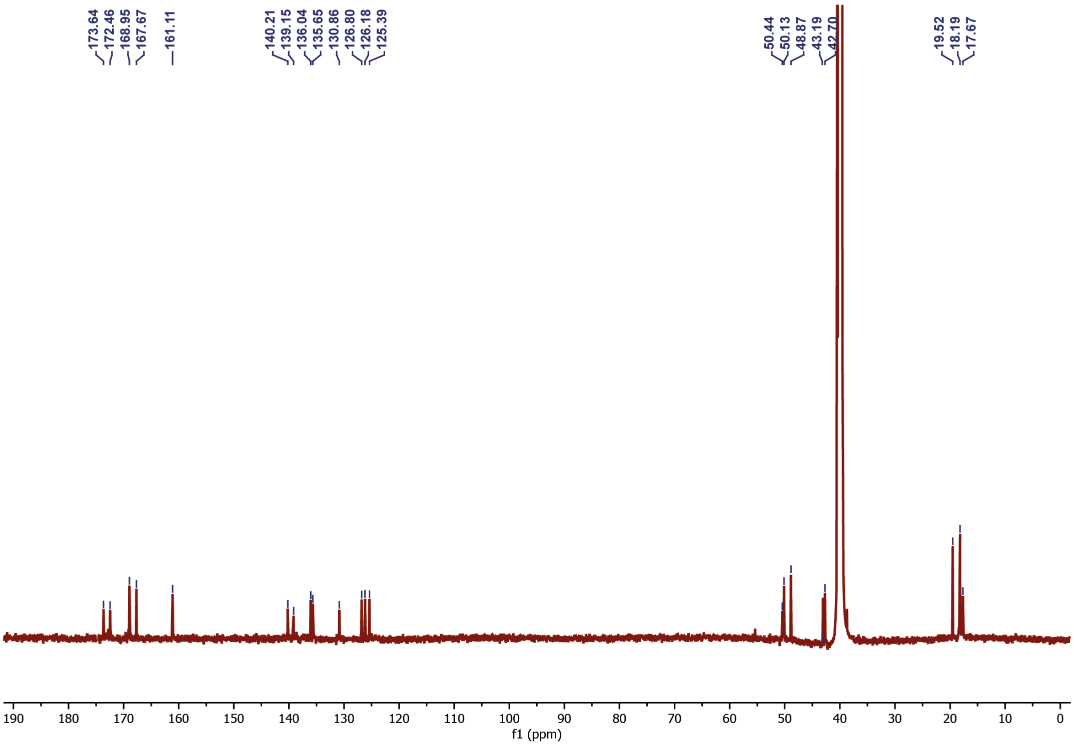

^{1}H-NMR and ^{13}C-NMR of compound **2** ($CDCl_3$)

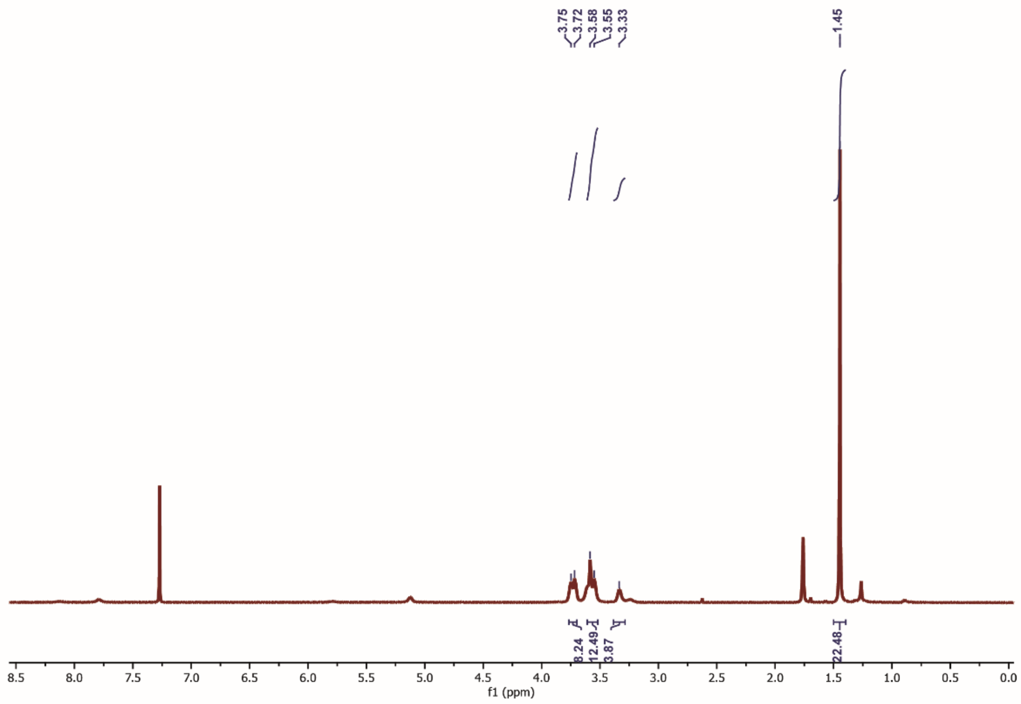

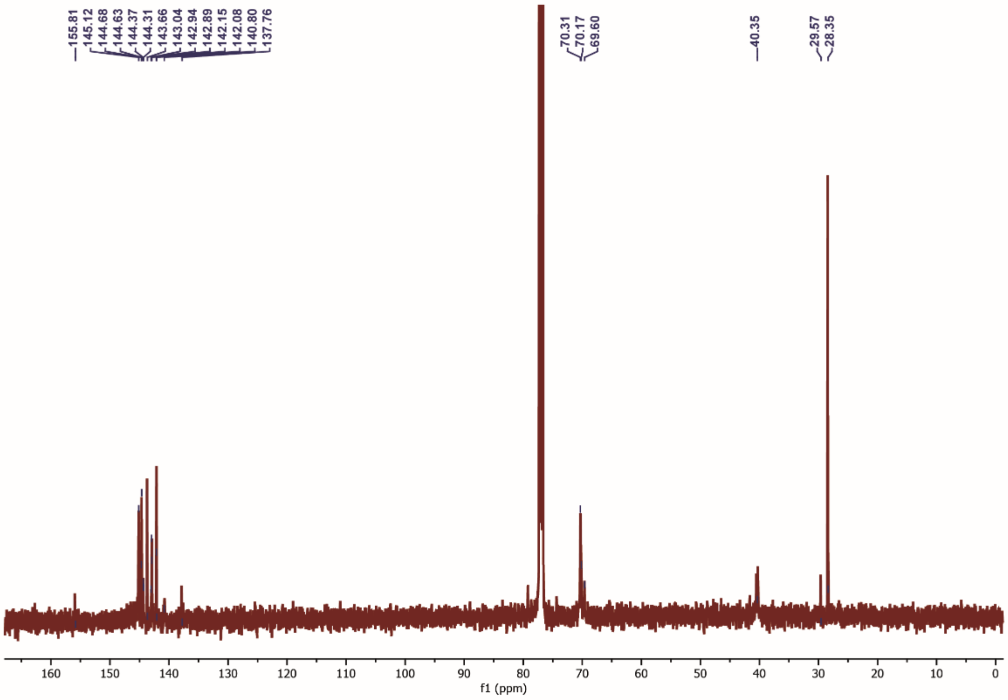

^{1}H-NMR and ^{13}C-NMR of compound **3** (MeOD-d_4)

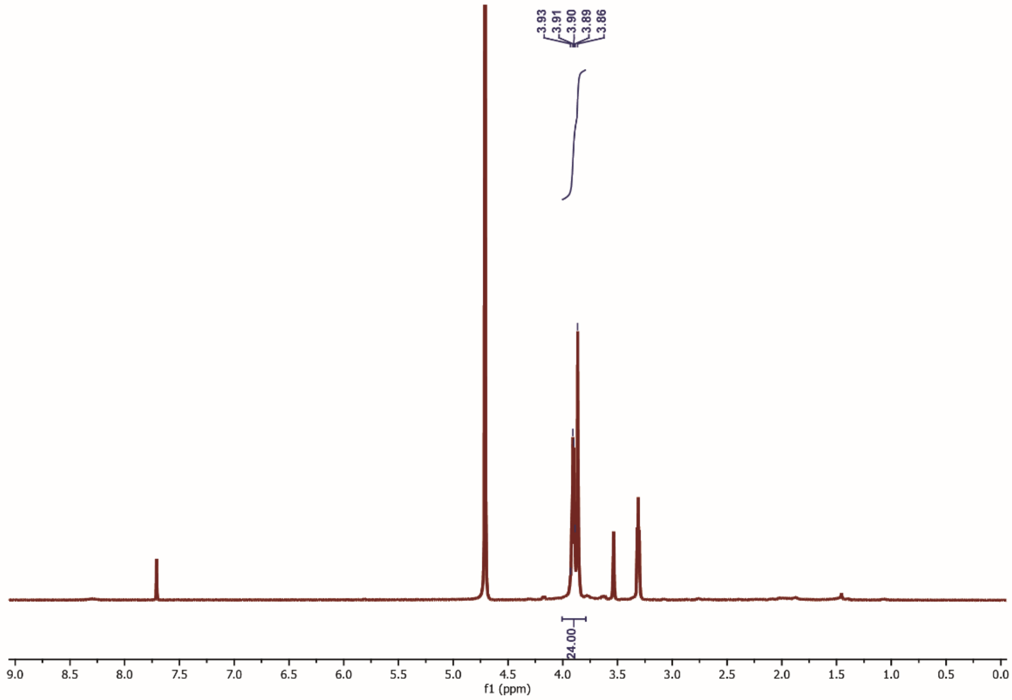

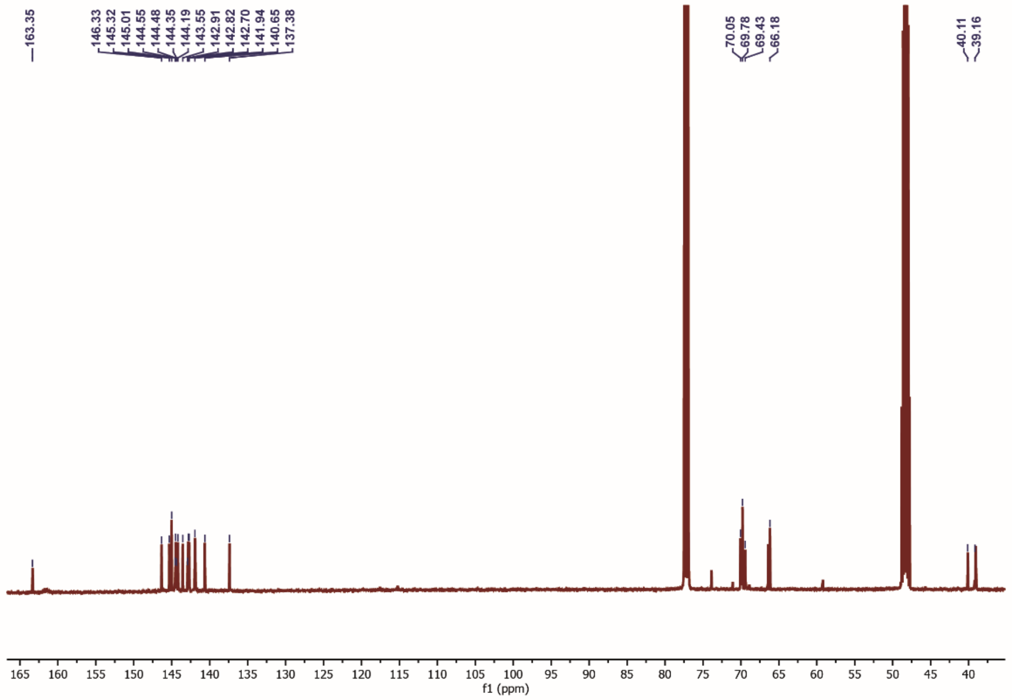

^{1}H-NMR and ^{13}C-NMR of compound **4** ($CDCl_3$)

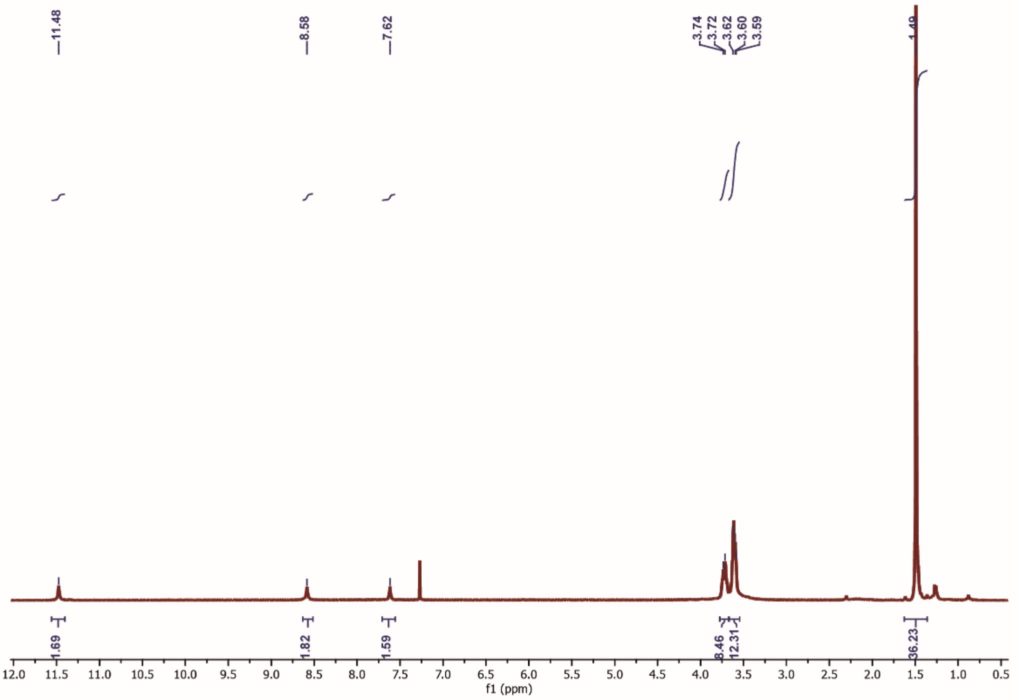

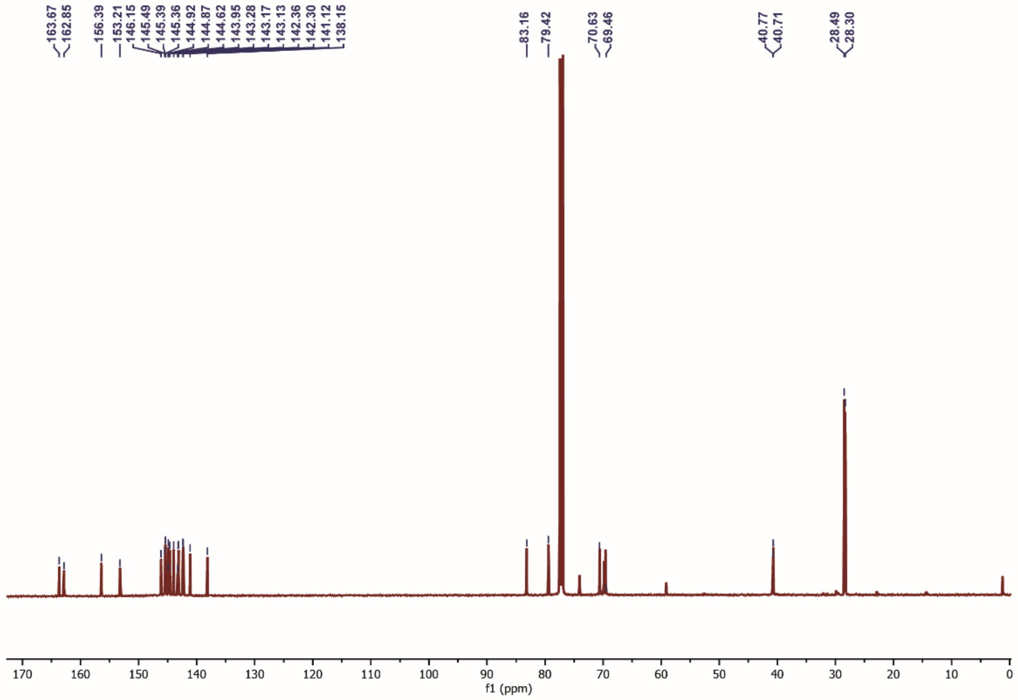

^{1}H-NMR and ^{13}C-NMR of compound **C_{60}MA** (DMSO-*d6*)

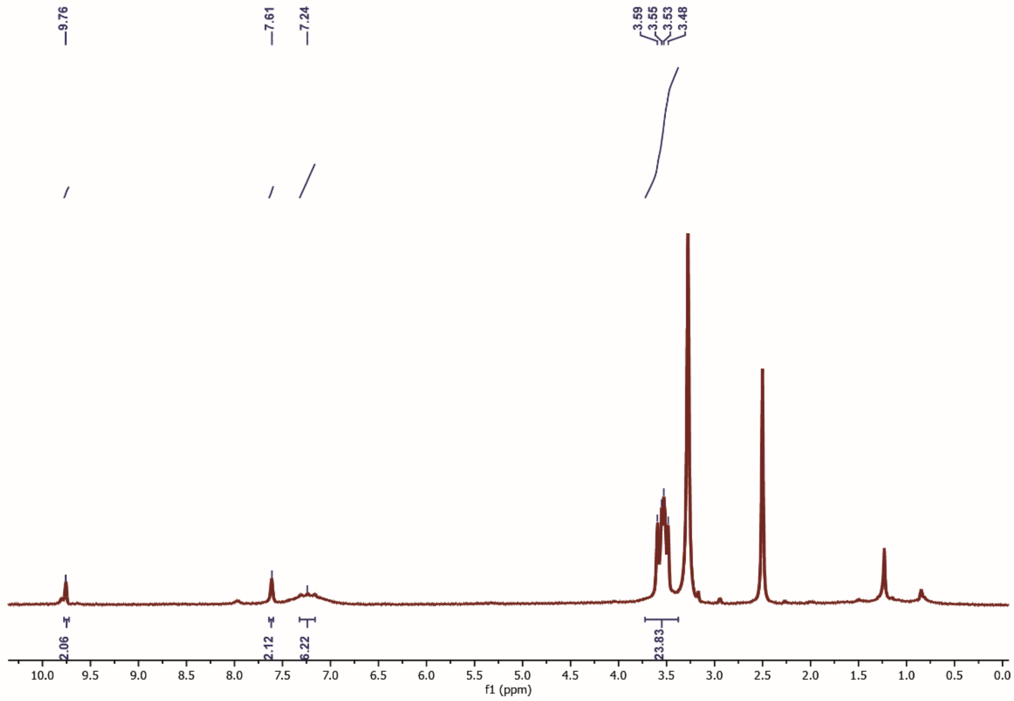

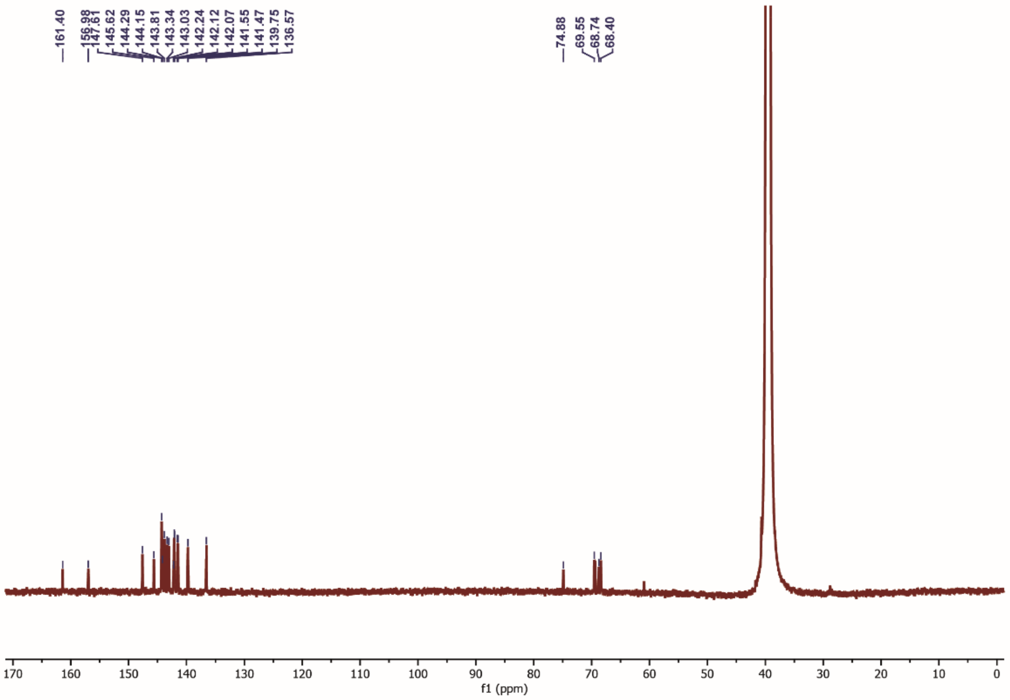

4. FP-TRMC and TAS measurements.

Nanosecond laser pulses from a Nd:YAG laser of Spectra-Physics INDI-HG(full width at half maximum ($\phi\Sigma\mu$) of 5—8 ns was used as an excitation light source, and the third harmonic generation (THG) (355 nm) were exposed to the solid films of **QT**, **QT:PBI**, and **QT:C$_{60}$MA**. The laser power density was set to 5.1 mJ cm^{-2} (9.1 × 10^{15} photons cm^{-2}). For TRMC measurements, the microwave frequency and power were set at approximately 9.1 GHz and 3mW, respectively, and the TRMC signal was evoluted in a diode (rise time < 1 ns), and output signal was led into a digital oscilloscope of Tektronix TDS 3032B. All experiments described above were conducted at room temperature. Reflected power change ratio ($\Delta P_r/P_r$) of microwave from the cavity in FP-TRMC apparatus is in relation with the total loss ($\Delta(1/Q)$) of microwave by the photo-induced transient species in the cavity as follows[1]:

$$\frac{\Delta P_{\mathrm{r}}}{P_{\mathrm{r}}} = \frac{\left(\frac{1}{Q}\right)}{\left(\frac{\Delta\omega}{\omega_0}\right)^2 + \left(\frac{1}{2Q}\right)^2}\,\Delta\left(\frac{1}{Q}\right) \qquad (1),$$

where, ω_0 and $\Delta\omega$ are the resonant frequency of 9.1 GHz and its shift by the photo-induced transient species. The loss and the frequency shift of the microwave are expressed as a function of complex conductivity ($\Delta\sigma_r + i\Delta\sigma_i$) of the transient species by:

$$\Delta\left(\frac{1}{Q}\right) - i\frac{2\Delta\omega}{\omega_0} = F\left(\Delta\sigma_{\mathrm{r}} + i\Delta\sigma_{\mathrm{i}}\right) \qquad (2),$$

where F is a calibration factor derived from the measurements of total loss of microwave in the cavity loaded with materials with well-known conductivity values. The value of $\Delta P_r/P_r$ will be proportional to the sum of the mobilities ($\Sigma\mu$) of charged species in case of negligibly small $\Delta\omega$:

$$\Delta\sigma_{\mathrm{r}} = N\phi\sum\mu = \mathrm{A}\frac{\Delta P_{\mathrm{R}}}{P_{\mathrm{R}}} \qquad (3),$$

where N, ϕ, and A are the number of absorbed photons, photo-carrier separation quantum yield, and a sensitivity factor (constant), respectively. Details in the sensitivity factor, A are described elsewhere.[2]

To determine the values of ϕ, we conducted transient optical absorption spectroscopy at 25 °C using solid film of deposited onto an identical quartz substrate to that in FP-

TRMC measurements.[3] Transmittance of excitation light pulses was measured by a PE25 power meter of Ophir Optoronics Ltd., leading to the > 99% absorbance of the films for the laser pulses. Time-dependent absorption spectral changes were monitored by Hamamatsu C7700 streak camera via a Hamamatsu C5094 spectrometer upon excitation of the film with 355 nm light pulses from an identical laser system for TRMC measurements. The excitation density was tuned at 1.8×10^{16} cm^{-2} photons per pulse. The streak scope images were averaged over 2500 images to correct a 2-dimensional time-wavelength correlation data of the transient absorption. The values of f were calculated on the assumption of balanced charges of holes and electrons on **QT** and **PBI** or **$\mathbf{C_{60}}$MA**, respectively. On the basis of the molar extinction coefficients of **PBI** radical anions ($\varepsilon^{\cdot-} = 7.4 \times 10^4$ $\mathrm{mol^{-1}dm^3cm^{-1}}$), the values of ϕ was determined as 6.0×10^{-4} in **QT:PBI** systems.

5. General method for the preparation of n/p-co-assembled nanostructures for UV-vis, CD, FT-IR and XPS spectroscopy, TEM imaging and FP-TRMC measurements.

In a typical experiment, 20 mL of 0.2 mM buffered aqueous solution of **QT** was annealed in the required conditions to generate each kind of nanofibers (depicted in the picture below). These solutions were mixed with 20 mL of 0.2 mM aqueous solution of **PBI** or **C_{60}MA** and allowed to set for 2 days in an orbital shaker at room temperature in the case of **QT-PBS** and **QT-TH**, or at 4 ºC in the case of **QT-ME**. For each batch, the obtained powder was centrifuged at high rpm rate (1 x 104 rpm for 10min) in a Falcon conical centrifuge tube to clean from salts and the excess of starting materials. The upper 75% of the supernatant was removed from the centrifugation tubes and around 20 mL of cleaned deionized water was added. The Falcon tube was shacked until a homogeneous dispersion was obtained and it was centrifuged again. This process was repeated until obtaining a colourless supernatant. Finally the dispersions were freeze-dried, obtaining 4 to 5 mg of each material. For UV-vis and CD each powder was dispersed in water and its spectra was recorded. In the case of XPS analysis, the samples were introduced in the apparatus as powder coated over a polycarbonate membrane. In the case of TEM imaging, 5 μL of well-dispersed sample in water was deposited on the carbon coated grid, allowed to settle/incubate for approximately one minute and blotted dry. For AFM, the same well-dispersed samples were spin coated on mica. Below a picture showing a batch of each **QT-**based supramolecular polymer is depicted. From left to right: **QT-PBS**; **QT-TH**; and **QT-ME** (the latter introduced in an ice-bath for stabilization of the metastable aggregate as previously indicated).

For SEM, a previous treatment of the formed n/p-co-assembled (**QT:PBI-TH** and **QT:C_{60}MA-TH**) was necessary in order to remove the occluded water without perturbing the structure of the materials: concentrated samples were fixed by an aqueous solution of glutaraldehyde and paraformaldehyde (2.5% and 4%, respectively) for 2 h. After washing several times with deionized water, sample dehydration was carried out by slow exchanging with a gradient of water-ethanol mixtures (30, 50, 70 up to 100% of ethanol) until the gel was in 100% ethanol. Samples were immersed in each solution for at least 10 min. The ethanol was removed by critical point drying.

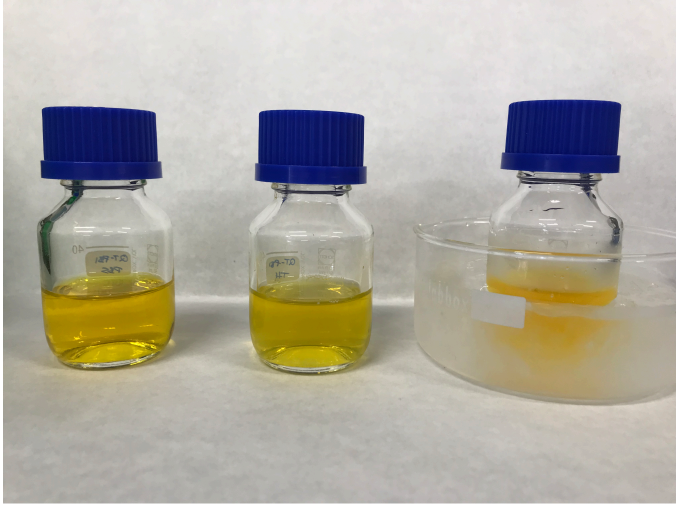

6. Supporting Figures

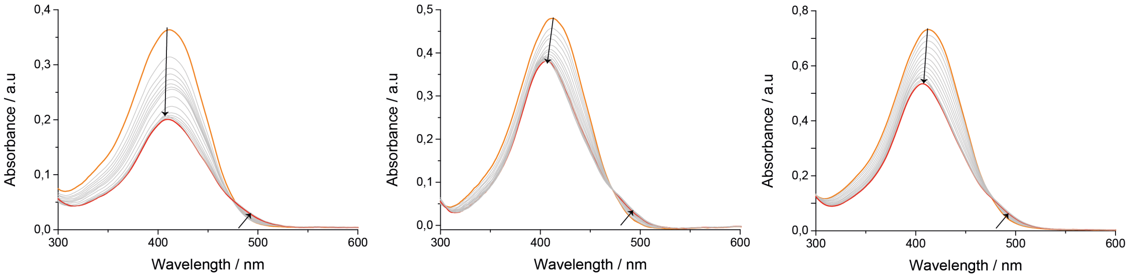

Figure S1. UV-vis spectra of **QT** (0.1 mM) in PBS buffer solution (pH 7.2) at different buffer's ionic strengths from the molecularly dissolved specie at 90 ºC (orange line) to 10 ºC (red line). From left to right: 10, 50 and 100 mM. Arrows are indicating the evolution of the signal.

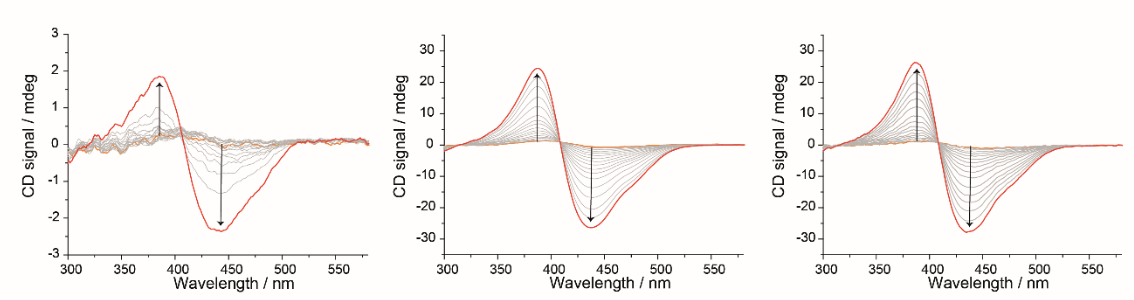

Figure S2. CD spectra of **QT** (0.1 mM) in PBS buffer solution (pH 7.2) at different buffer's ionic strengths from the molecularly dissolved specie at 90 ºC (orange line) to 10 º C (red line). From left to right: 10, 50 and 100 mM. Arrows are indicating the evolution of the signal.

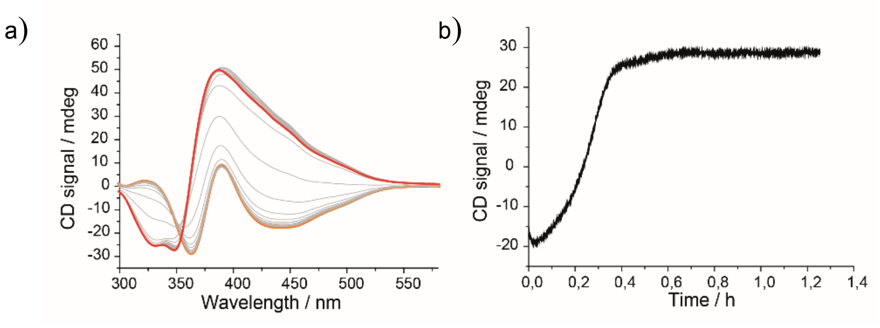

Figure S3. (a) CD signal evolution over time at room temperature of a fresh solution of **QT** in citric acid/sodium citrate buffer solution (I = 10 mM) from the metastable (orange line) to the thermodynamic (red line) aggregates. (b) Monitorization of the CD signal at 370 nm derived from previous experiment.

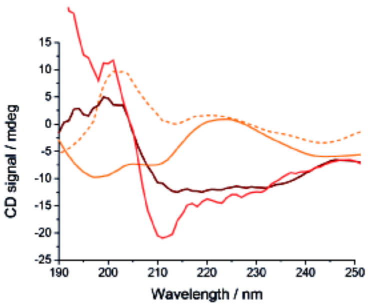

Figure S4. CD signal in the peptide region for **QT** (c = 0.1 mM) in PBS buffered solution (I = 50 mM) at 90 ºC (molecularly dissolved specie, orange dashed line) and 10 ºC (orange solid line) and in citric/sodium citrate buffered solution (I = 10 mM) for the metastable (red solid line) and the thermodynamic aggregates (brown solid line).

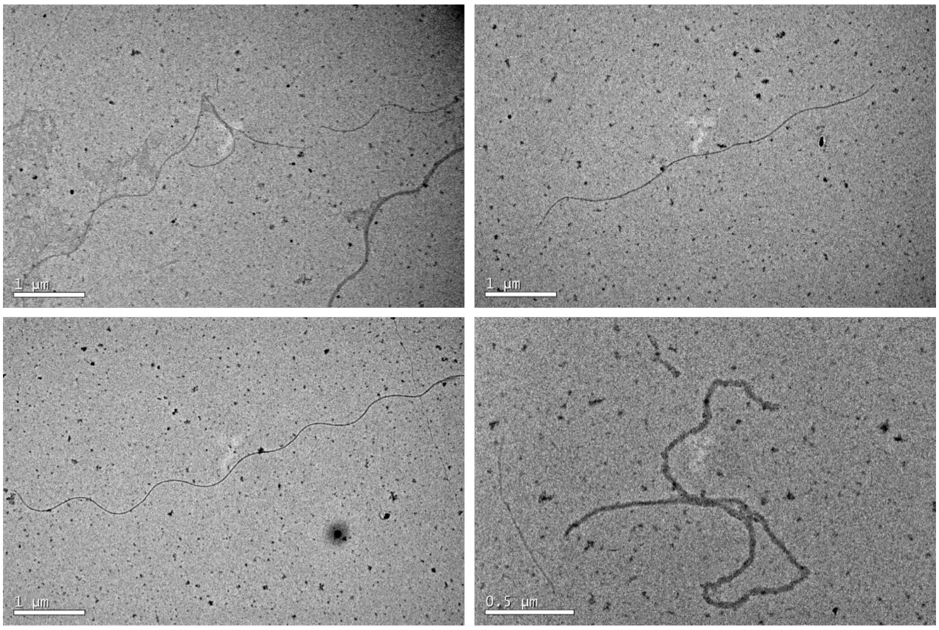

Figure S5. Different TEM images (taken from various sections of the grid) of **QT** (0.1 mM) in PBS buffer solution (pH 7.2, I = 10 mM) showing long twisted fibers. Scale bar: 1 µm.

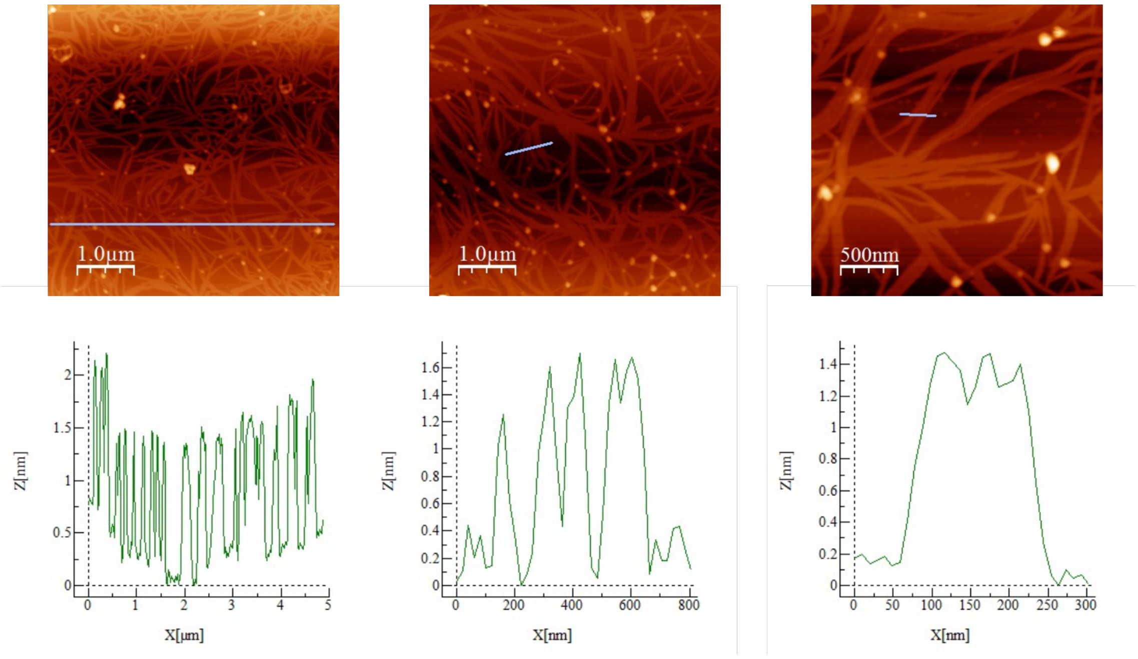

Figure S6. AFM images (up) and height profiles across the blue lines (down) of **QT-PBS** (*c* = 0.1 mM) in PBS buffer solution (pH 7.2, *I* = 10 mM). Sample was drop casted on mica substrate and vacuum dried. Images showed bundles of fibers with homogeneous height profiles of around 1.5 nm.

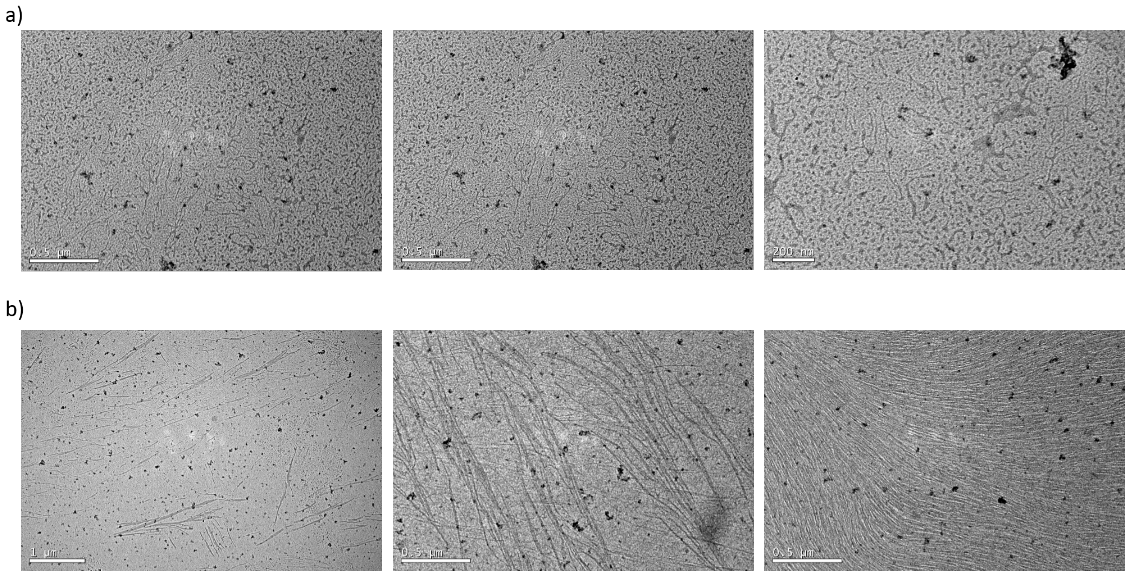

Figure S7. Different TEM images (taken from various sections of the grid) of **QT** (0.1 mM) in citric acid/sodium citrate buffer solution (pH 3.6, I = 10 mM) in metastable conditions freshly prepared (a) and after 15 min at room temperature. Small nanoparticles and very short fiber like aggregates can be observed when the sample is freshly prepared; however after 15 min this aggregates have considerably evolve, yielding nanofibers that in some regions appeared as a highly oriented film that is coating a big area of the grid (b, image on the right).

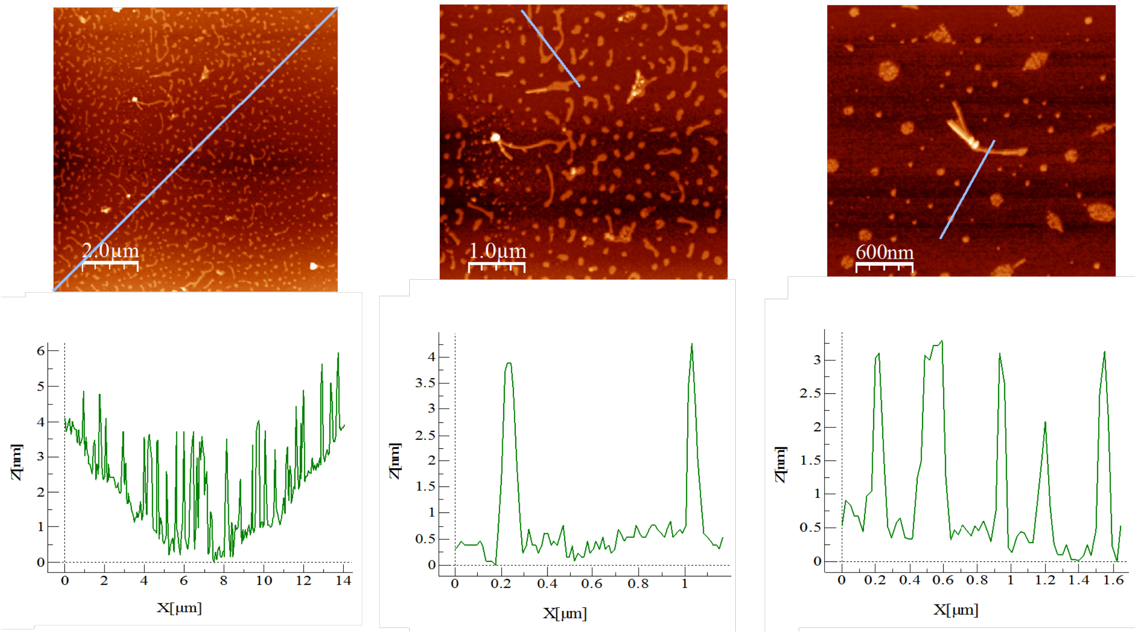

Figure S8. AFM images (up) and height profiles across the blue lines (down) of **QT-ME** (*c* = 0.1 mM) in citric acid/sodium citrate buffer solution (pH 3.6, *I* = 10 mM) in metastable conditions. Sample was spin coated on mica substrate and rapidly vacuum dried to avoid aggregates to evolve while air drying. Images show small nanoparticles and some short fibers as observed in TEM. Height profiles show a homogeneous height distribution of around 3 nm.

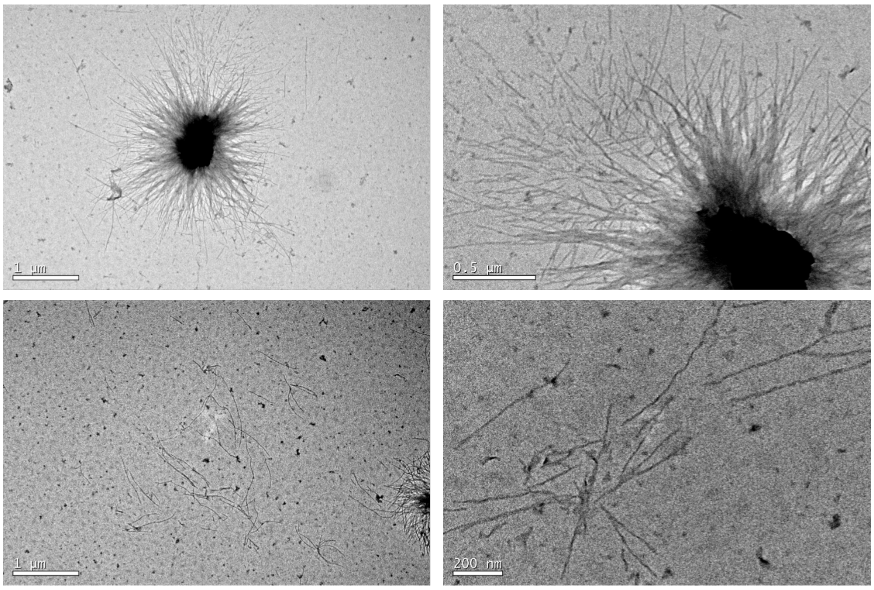

Figure S9. Different TEM images (taken from various sections of the grid) of **QT** (0.1 mM) in citric acid/sodium citrate buffer solution (pH 3.6, I = 10 mM) in thermodynamic equilibrium showing bundles of gathered fibers (up) and some isolated fibers in other areas (down).

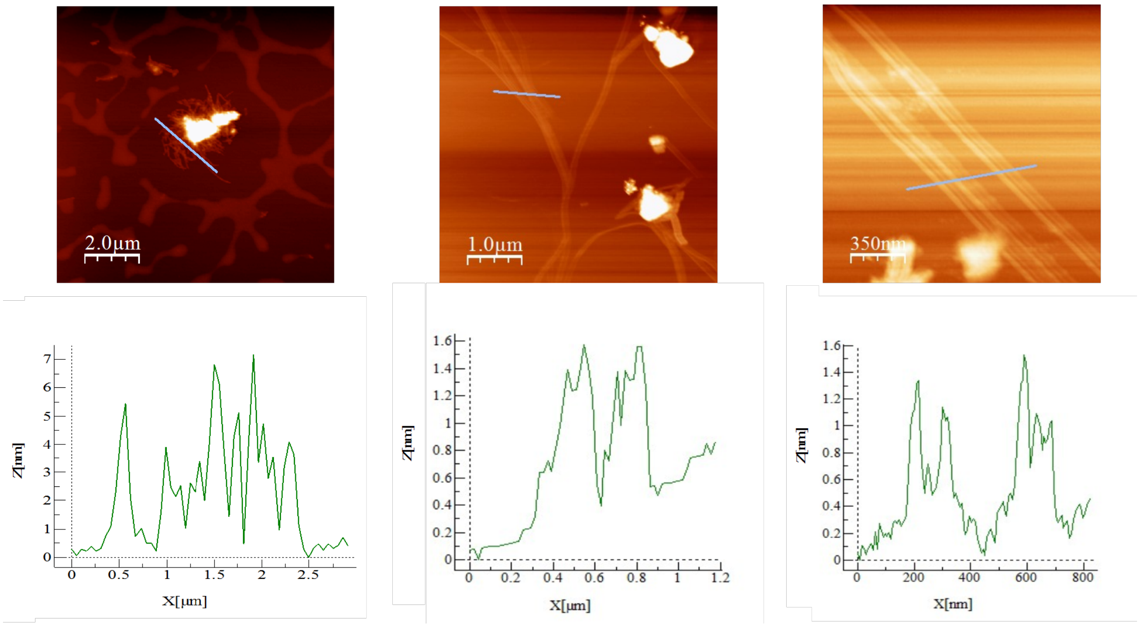

Figure S10. AFM images (up) and height profiles across the blue lines (down) of **QT-TH** (c = 0.1 mM) in citric acid/sodium citrate buffer solution (pH 3.6, I = 10 mM) under thermodynamic equilibrium. Images show bundles of gathered fibers and some isolated fibers in other areas as observed in TEM. Height profiles show a homogeneous height distribution of about 1.5 nm, which increases when fibers appear as bundles.

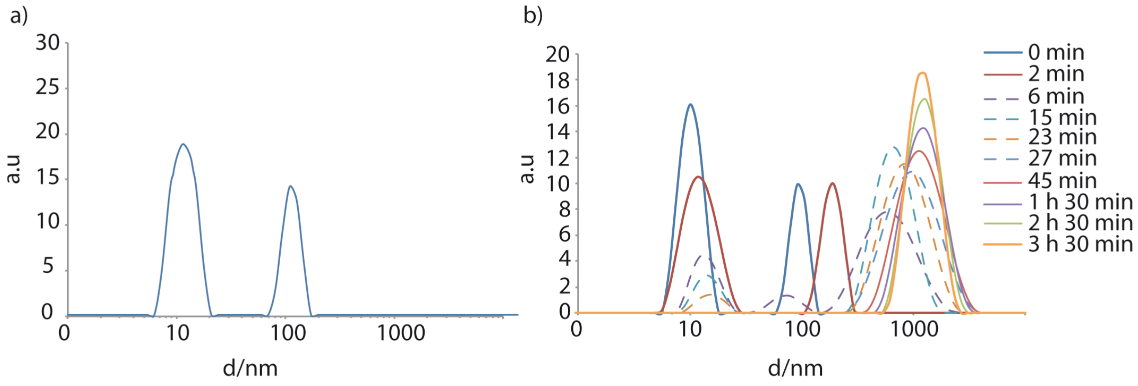

Figure S11. Dynamic ligth scattering data of **QT-PBS** (*c* = 0.1 mM, *I* = 50 mM) (a) and **QT** (*c* = 0.1 mM) in citric acid/sodium citrate buffer (*I* = 10 mM) (b). In figure b, we present the evolution from the initial out of equilibrium state, **QT-ME**, to the final thermodynamically stable state, **QT-TH**, after ~45 min. This fact is in concordance with the evolution observed using spectroscopical (UV-vis and CD) and microscopy (TEM and AFM) techniques.

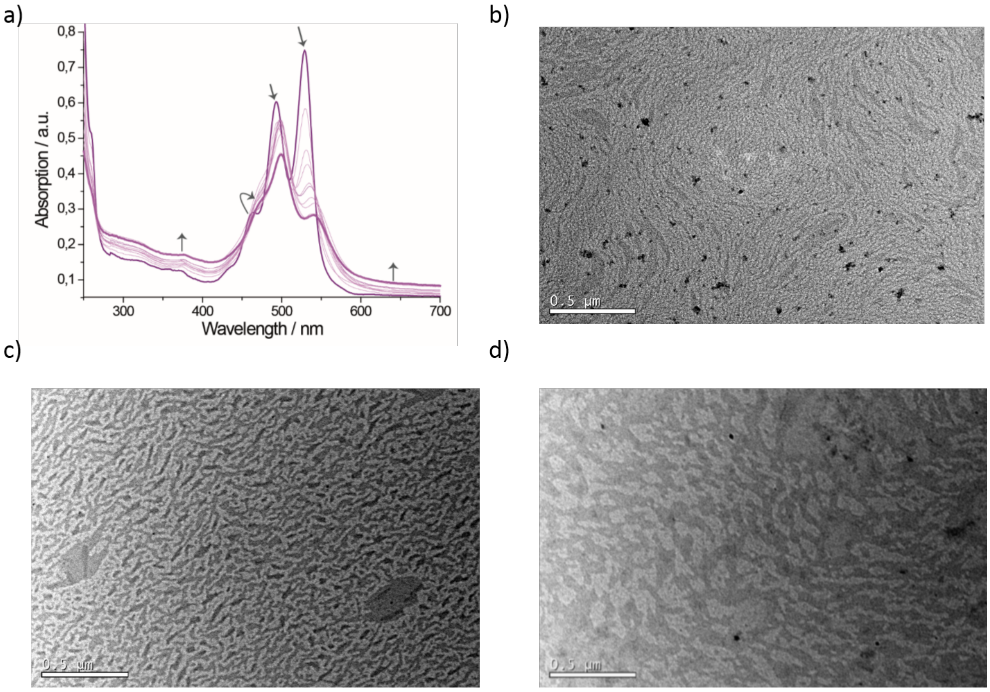

Figure S12. UV-vis spectra of **PBI** (a) from DMSO to water **(**c = 0.1 mM**)** and TEM images of each aggregate in water (b), PBS buffer (c) and citric acid/sodium citrate buffer (d). Arrows indicate the evolution of the absorption bands with increasing amounts of water.

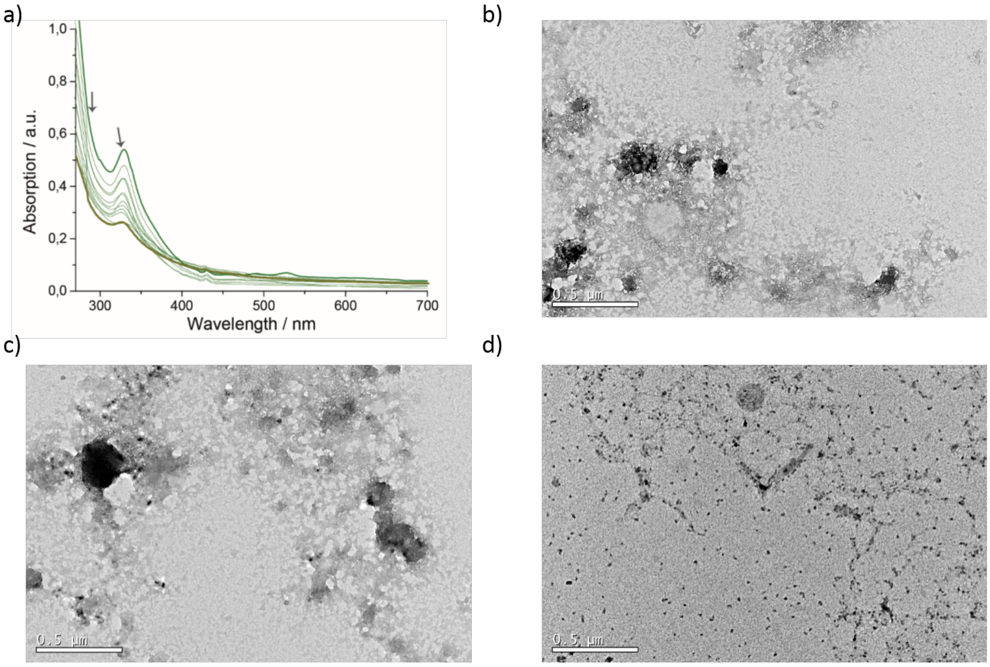

Figure S13. UV-vis spectra **C_{60}MA** (a) from DMSO to water **(**c = 0.1 mM**)** and TEM images of each aggregate in water (b), PBS buffer (c) and citric acid/sodium citrate buffer (d). Arrows indicate the evolution of the absorption bands with increasing amounts of water.

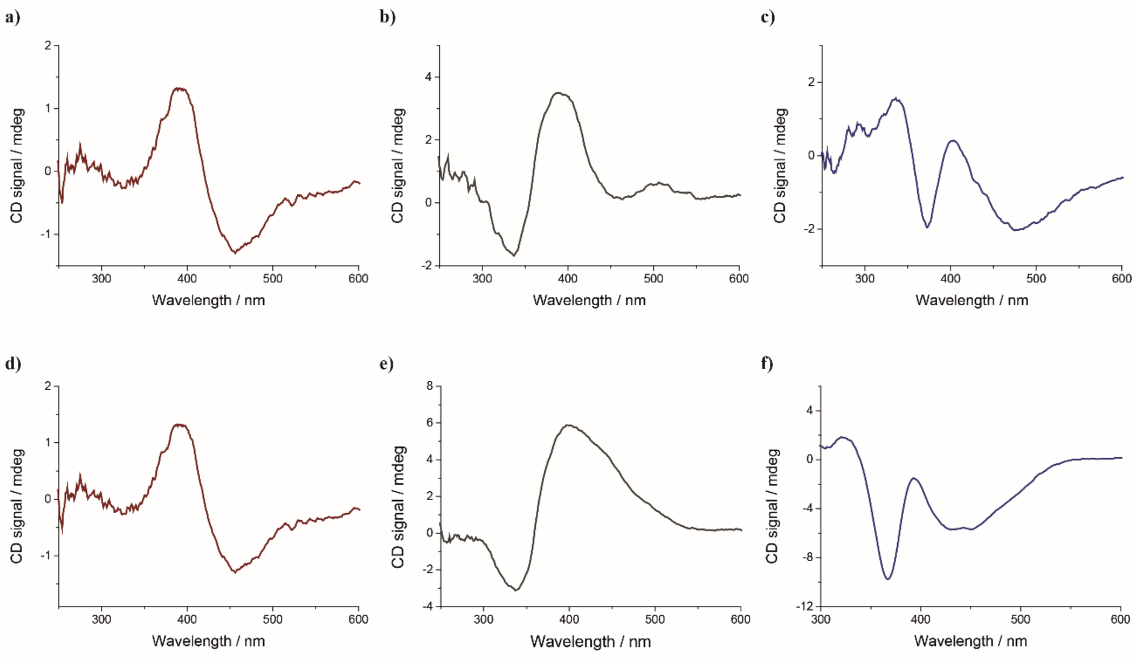

Figure S14. CD signal of the n-/p-materials dispersed in water. **QT:PBI** (a) and **QT:C_{60}MA** (d) from PBS solution; **QT:PBI** (b) and **QT:C_{60}MA** (e) from citric acid/sodium citrate buffer in thermodynamic conditions; **QT:PBI** (c) and **QT:C_{60}MA** (f) from citric acid/sodium citrate buffer under non-equilibrium conditions. Note that the CD profile corresponds to the former **QT** nanofibers, although signal intensity is not comparable due to the scattering of the dispersion of the hybrid materials.

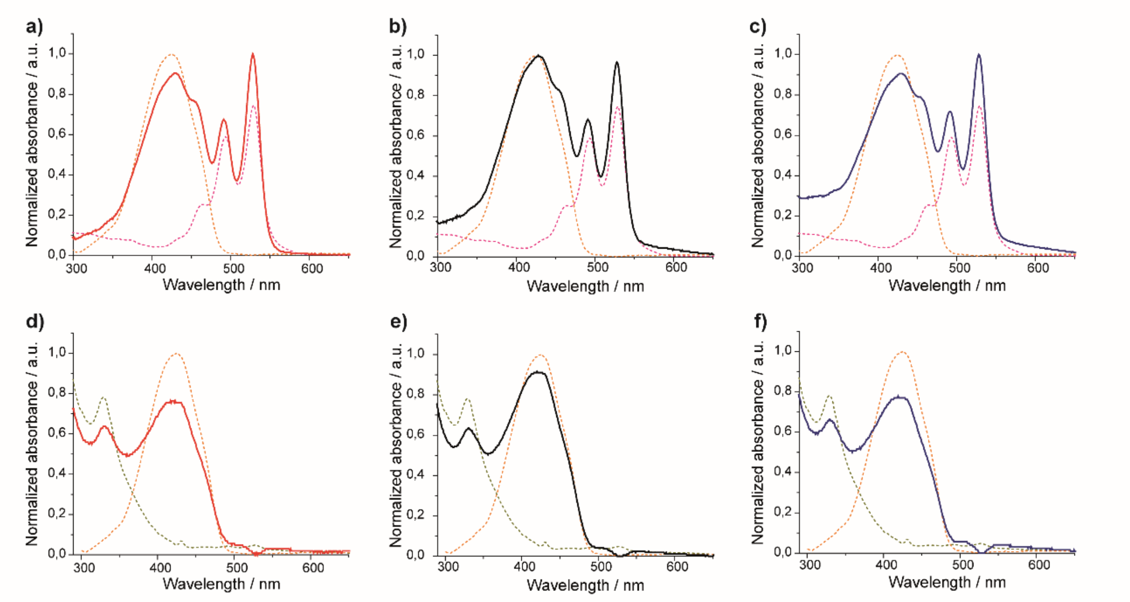

Figure S15. UV spectra of the denatured n-/p materials in DMSO for **QT**:**PBI** in PBS (a), and in citric acid/sodium citrate buffer under thermodynamic conditions (b) and kinetic conditions (c); for **QT**:**C$_{60}$MA** in PBS (d), and in citric acid/sodium citrate buffer under thermodynamic conditions (e) and kinetic conditions (f). Dash lines correspond to molecularly dissolved **QT** (orange), **PBI** (pink) and **C$_{60}$MA** (green) (c = 0.1 mM) in DMSO, for comparison.

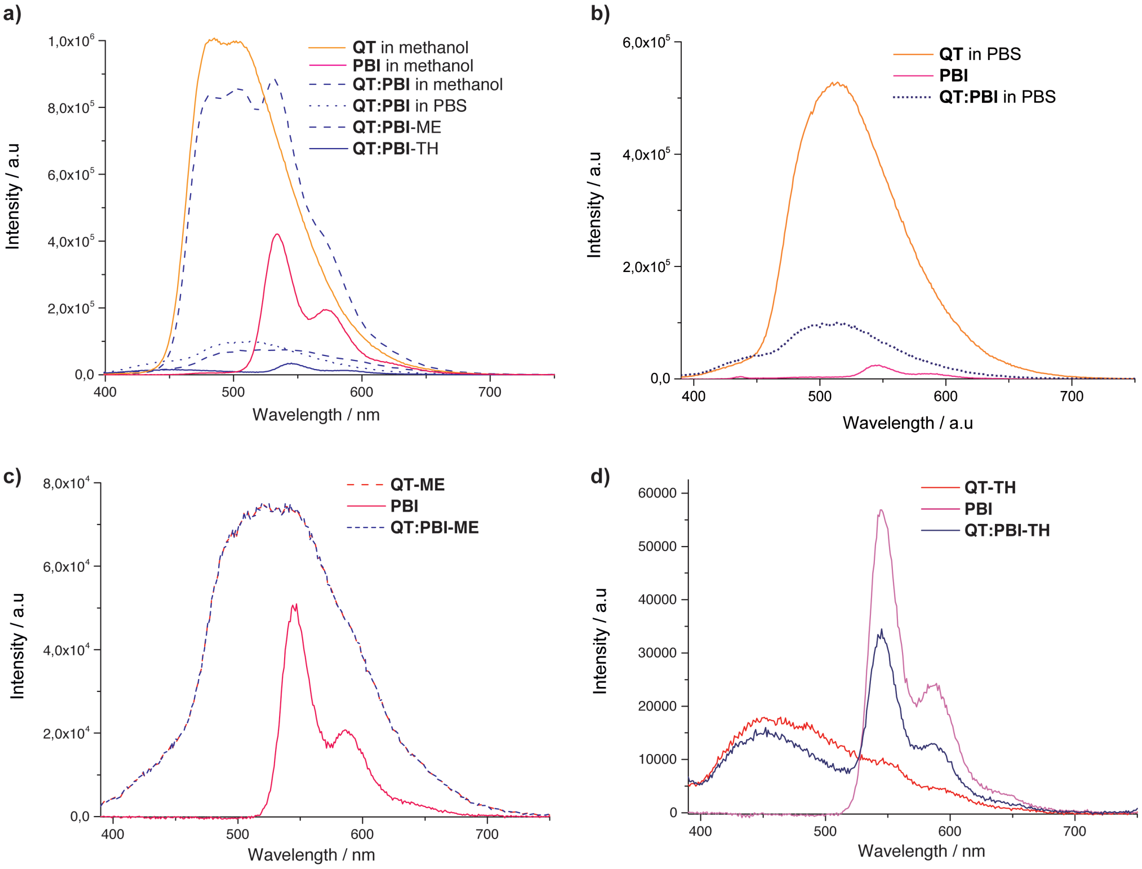

Figure S16. Emission spectra of **QT** (orange solid line), **PBI** (pink solid line), and **QT**:**PBI** co-assembled in methanol (black dash line), PBS (blue dot line) and in citric acid/sodium citrate buffer under kinetic conditions (blue dash line) and thermodynamic conditions (blue solid line) (a). Comparative emission spectra of building block **QT**, **PBI** and **QT:PBI** co-assembled under PBS (b) and in citric acid/sodium citrate buffer under kinetic conditions (c) and thermodynamic conditions (d). (λ_{exc}= 380 nm)

Table S1. Estimated values for the quantification of guanidinium-like amines and the rest of the amine moieties for different **QT – PBI/C$_{60}$MA** ratios and the depiction of these ratios, 1:1 (top), 1:2 (middle) and 2:1 (bottom)

	Terminal guanidinium amines	Other amines
1:1	22 %	78 %
2:1	31 %	69 %
1:2	14 %	86 %

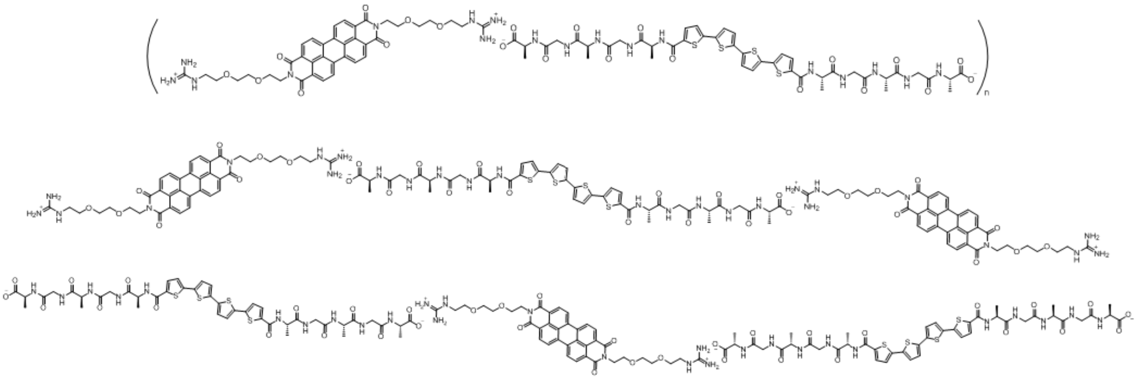

Table S2. Experimental values extracted from the deconvolution of the high-resolution spectra of the N-1s region which allowed the determination of the population of electronically distinct N amines with higher binding energy than the rest of amines.

SAMPLE	**TERMINAL GUANIDINIUM AMINES**		**OTHER AMINES**	
	Quantification	Position / eV	Quantification	Position / eV
QT-PBI-PBS	21.15	399.76	78.85	399.05
QT-C$_{60}$MA-PBS	22.75	400.05	77.25	399.85
QT-PBI-TH	22.94	400.39	77.06	400.08
QT-C$_{60}$MA-TH	21.82	399.79	78.18	399.59
QT-PBI-ME	20.22	400.01	79.78	399.72
QT-C$_{60}$MA-ME	19.55	399.81	80.45	399.54

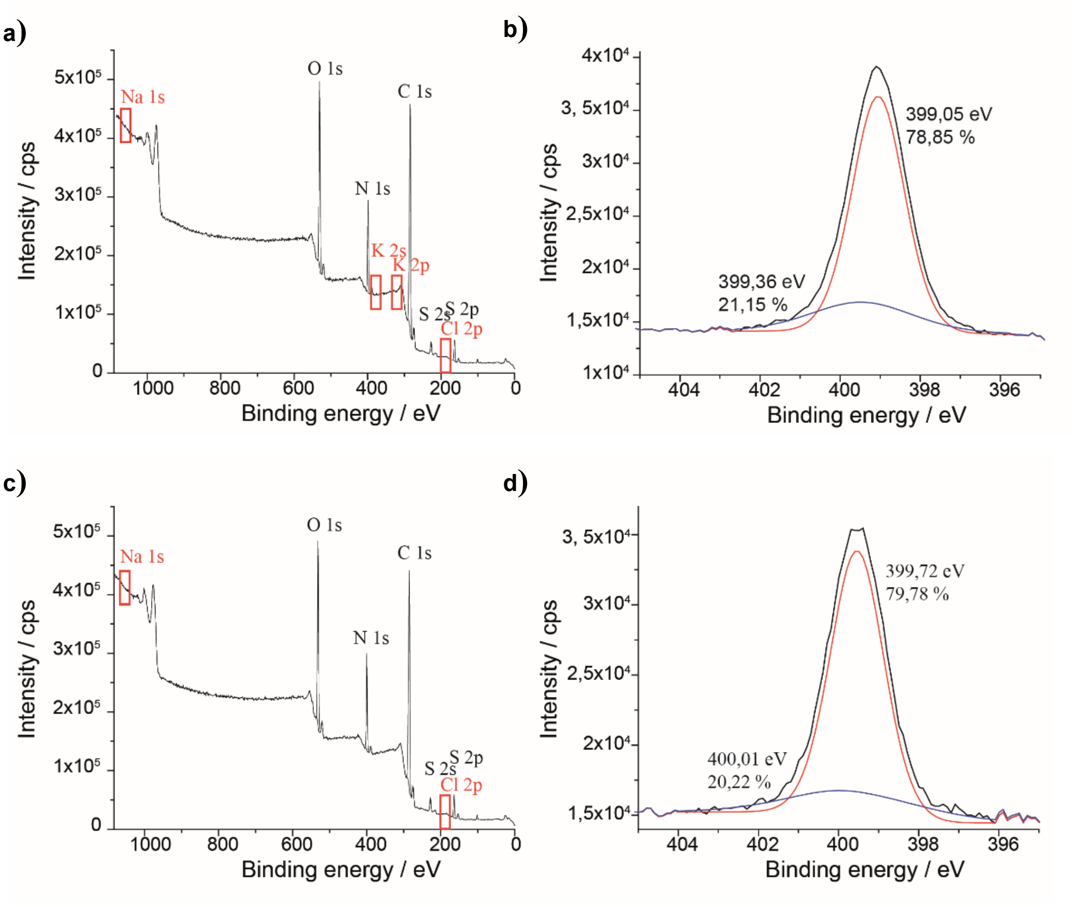

Figure S17. XPS survey spectra of a solid sample **QT:PBI** obtained in different conditions; in PBS (a,b), and in citric acid/sodium citrate buffer under kinetic (c-d) conditions. (Left) Full spectrum; (Right) High-resolution XPS spectrum of the N-1s region; Gaussian deconvolution of the N-1s signal determines the populations of electronically distinct N atoms. Note that this deconvolution demonstrates the quantitative ionic interactions between **QT** and **PBI** at the molecular lever (1:1) in all cases

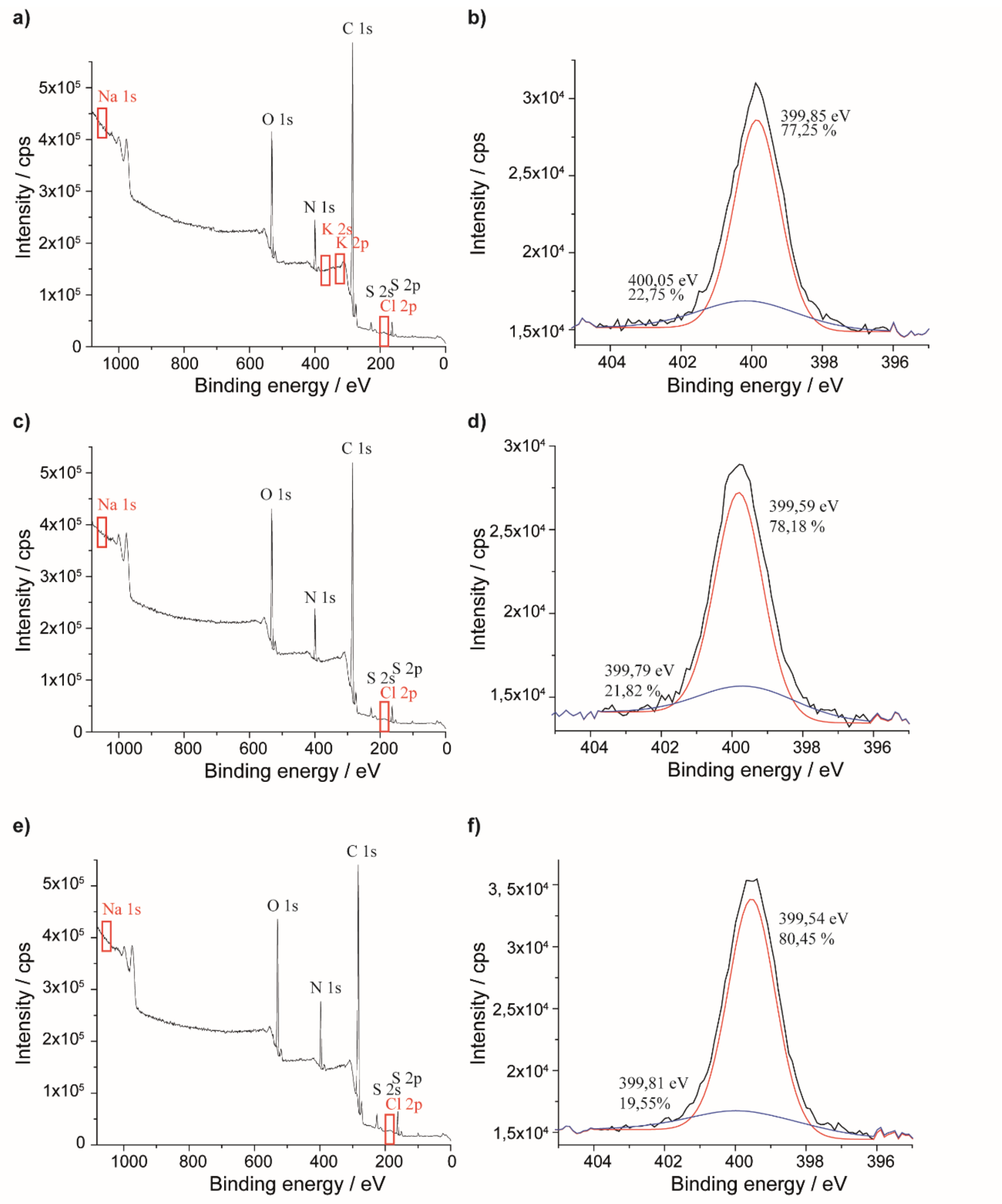

Figure S18. XPS survey spectra of a solid sample **QT**:**C_{60}MA** obtained in different conditions; in PBS (a,b) and in citric acid/sodium citrate buffer under thermodynamic (c,d) and kinetic (e-f) conditions. (Left) Full spectrum; (Right) High-resolution XPS spectrum of the N-1s region; Gaussian deconvolution of the N-1s signal determines the populations of electronically distinct N atoms. Note that this deconvolution demonstrates the quantitative ionic interactions between **QT** and **C_{60}MA** at the molecular lever (1:1) in all cases.

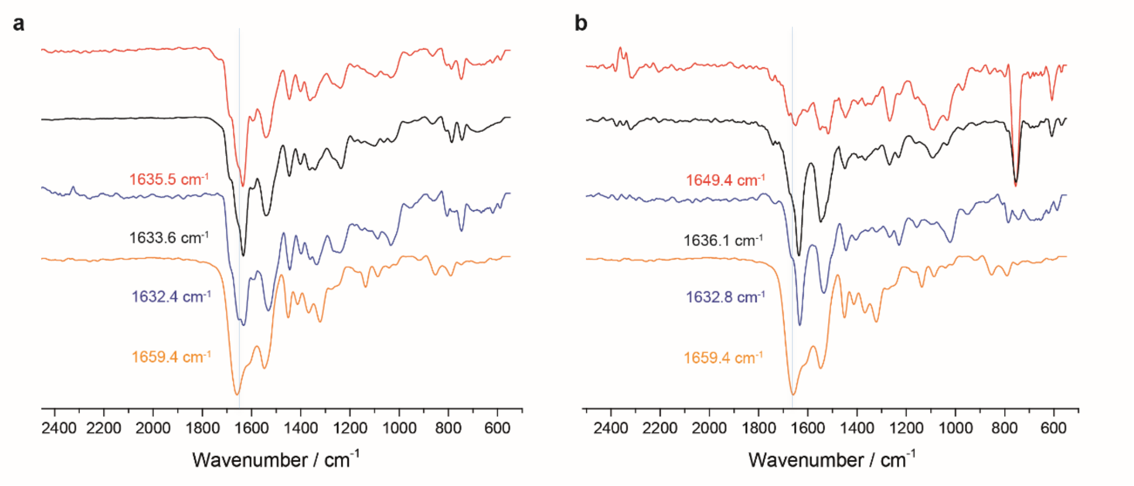

Figure S19. FTIR spectra of **QT** (orange) and the n/p-materials in the carbonyl-streching area. **QT:PBI** (a) and **QT**:**C$_{60}$MA** (b) in PBS (red), and in citric acid/sodium citrate buffer under thermodynamic (balck) and out of equilibrium (blue) conditions.

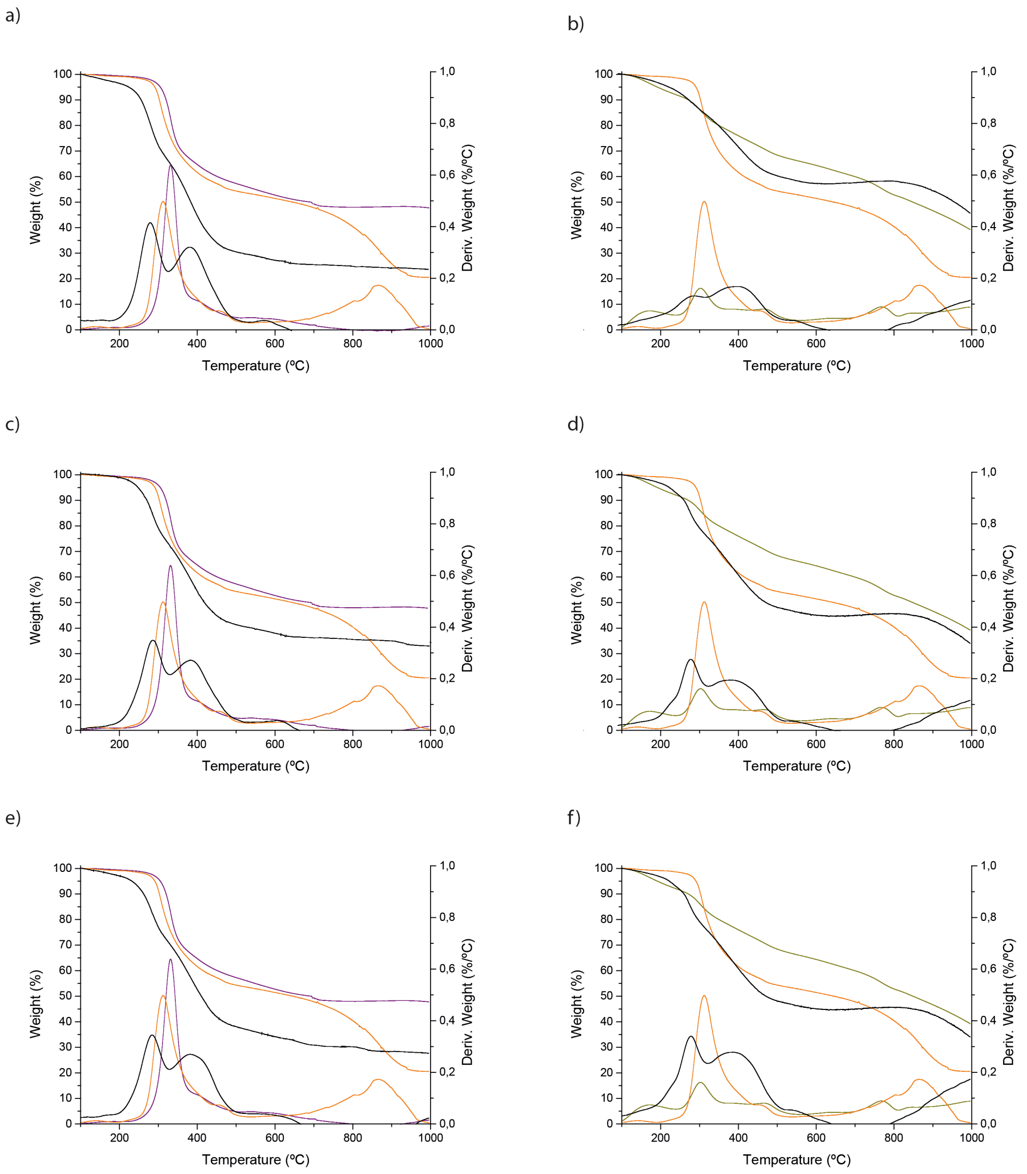

Figure S20. TGA analysis of the coassemblies and their corresponding former building blocks showing the weight loss and the first derivative. Black solid lines correspond to each coassembled material and orange, pink and green lines correspond to **QT**, **PBI** and **C_{60}MA** building blocks, respectively. **QT:PBI-PBS** (a) and **QT:C_{60}MA-PBS** (b) from PBS solution; **QT:PBI-TH** (c) and **QT:C_{60}MA-TH** (d) from citric acid/sodium citrate buffer in thermodynamic conditions; **QT:PBI-ME** (e) and **QT:C_{60}MA-ME** (f) from citric acid/sodium citrate buffer under out of equilibrium conditions.

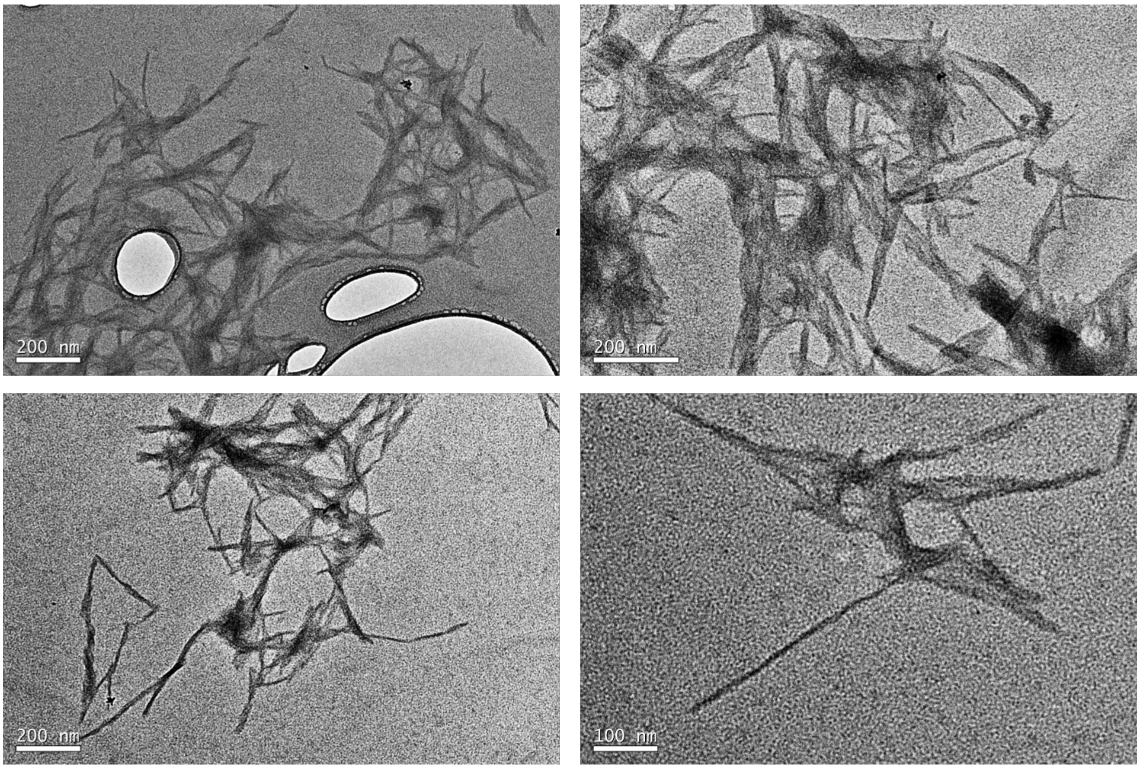

Figure S21. TEM images (taken from various sections of the grid) of **QT:PBI-PBS** coassemblies from previously equilibrated solutions of **QT** in PBS buffer solution and **PBI** in MiliQ water.

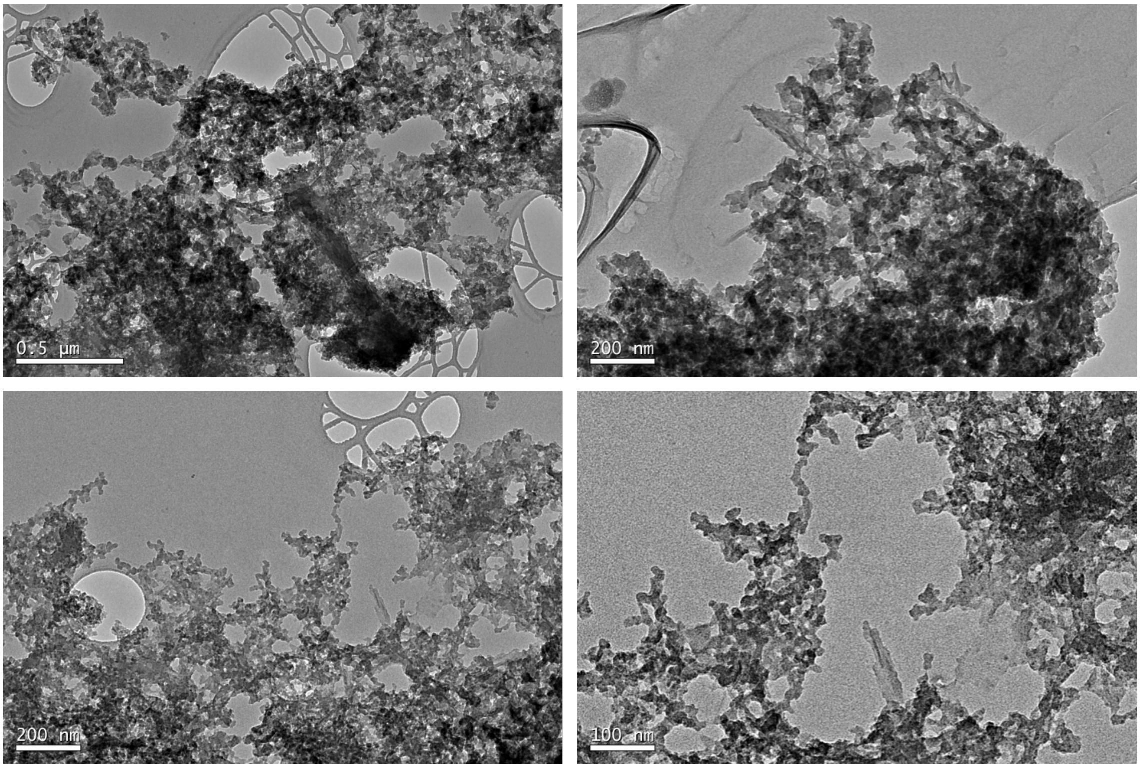

Figure S22. TEM images (taken from various sections of the grid) of **QT:C$_{60}$MA-PBS** coassemblies from previously equilibrated solutions of **QT** in PBS buffer solution and **C$_{60}$MA** in MiliQ water.

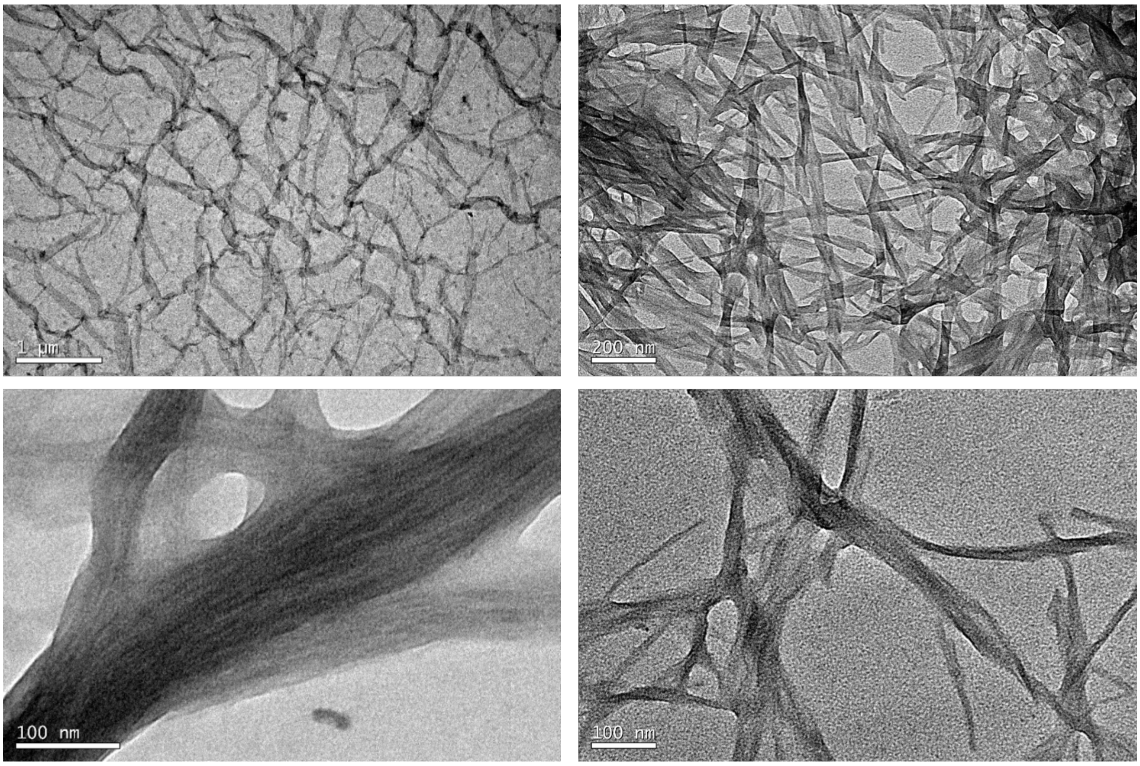

Figure S23. TEM images of **QT:PBI-TH** coassemblies from previously equilibrated solutions of **QT** in citric acid/sodium citrate buffer solution under thermodynamic conditions and **PBI** in MiliQ water.

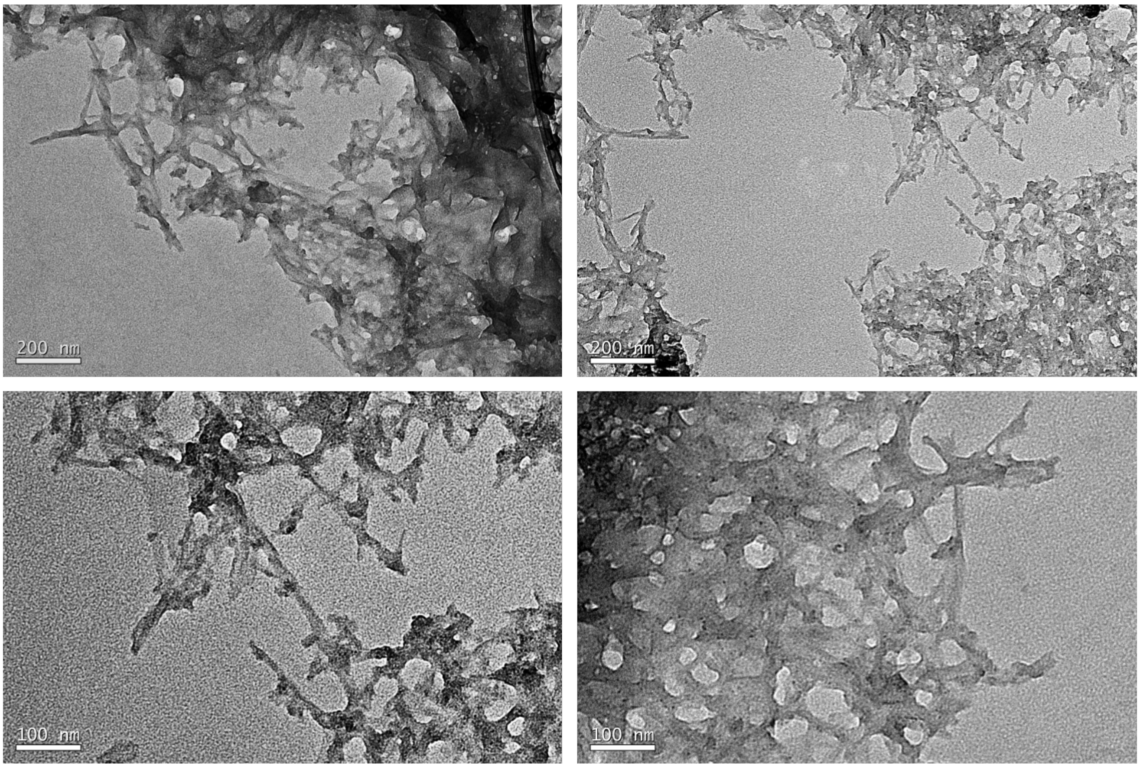

Figure S24. TEM images (taken from various sections of the grid) of **QT:C$_{60}$MA-TH** coassemblies from previously equilibrated solutions of in citric acid/sodium citrate buffer solution under thermodynamic conditions and **C$_{60}$MA** in MiliQ water.

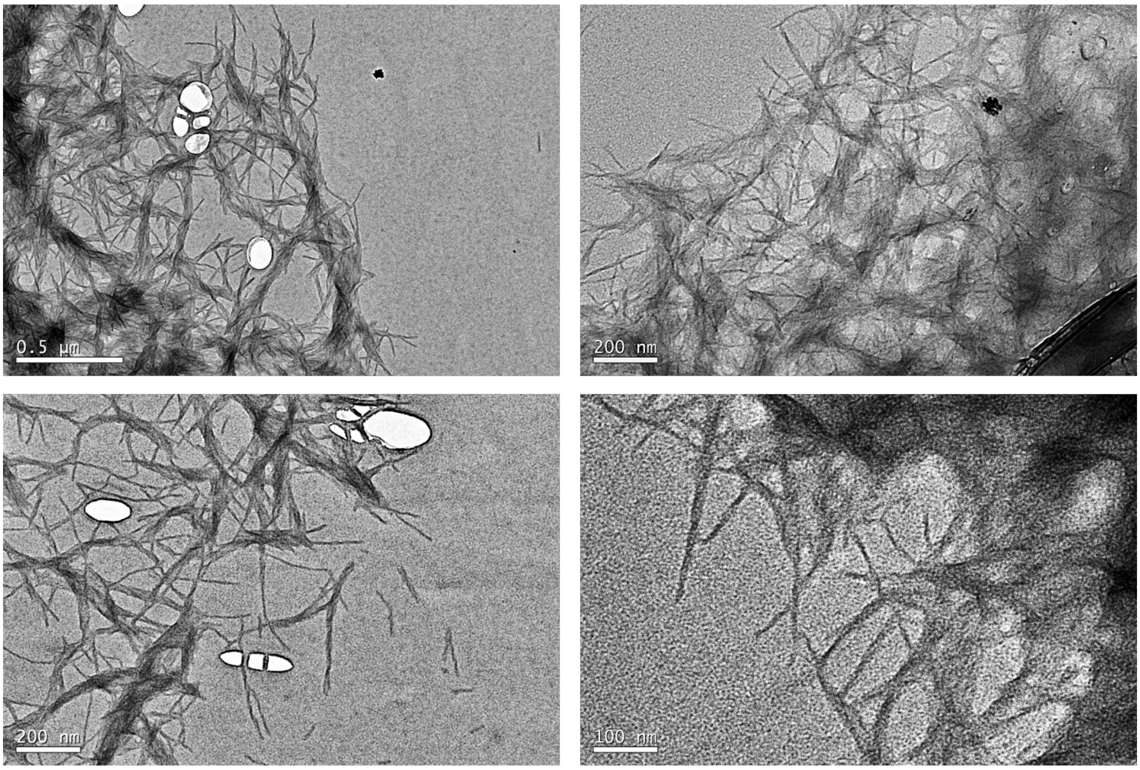

Figure S25. TEM images (taken from various sections of the grid) of **QT:PBI-ME** coassemblies from previously equilibrated solutions of **QT** in citric acid/sodium citrate buffer solution under non-equilibrium conditions and **PBI** in MiliQ water.

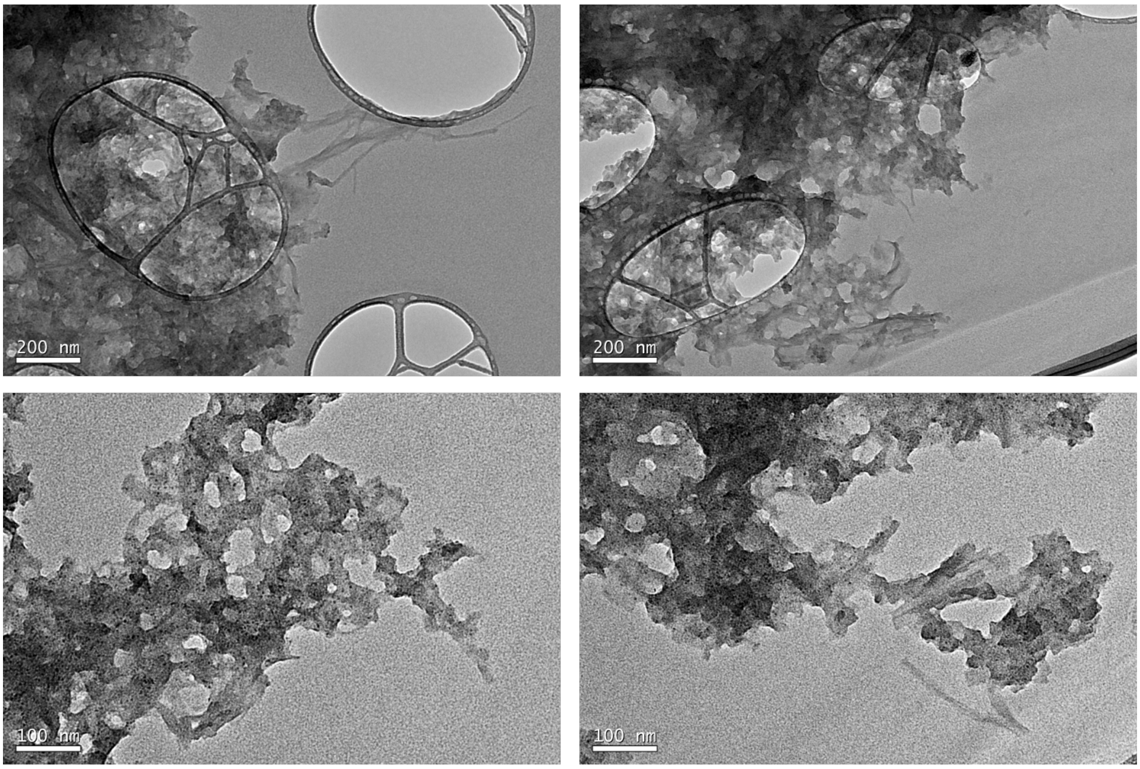

Figure S26. TEM images (taken from various sections of the grid) of **QT:C$_{60}$MA-ME** coassemblies from previously equilibrated solutions of in citric acid/sodium citrate buffer solution under thermodynamic conditions and **C$_{60}$MA** in MiliQ water.

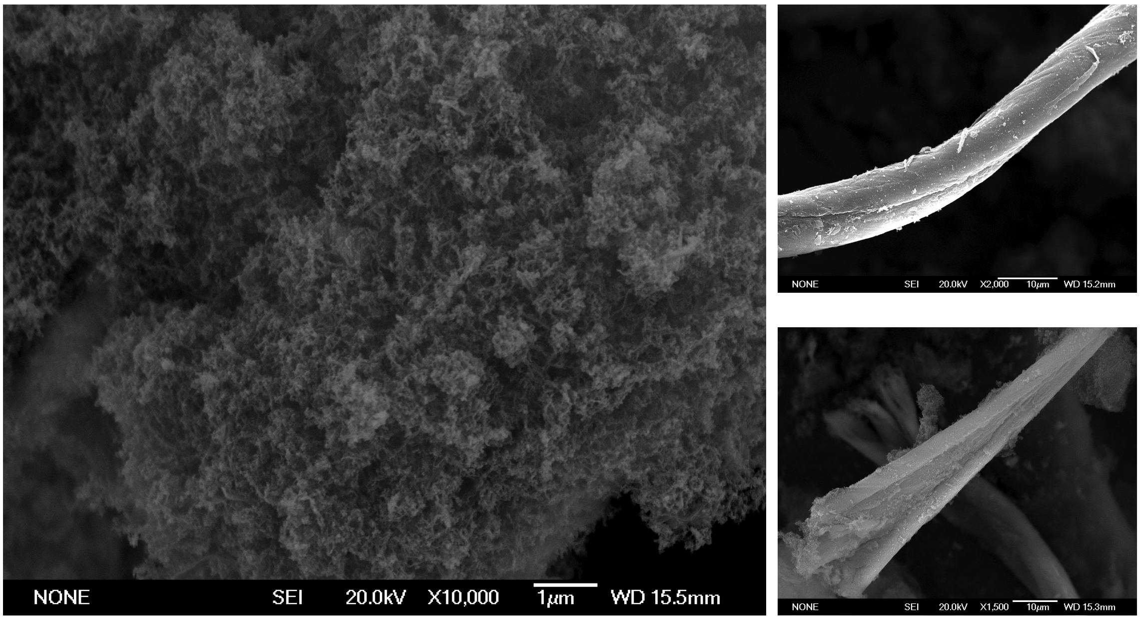

Figure S27. SEM images of **QT:PBI-TH** coassemblies, dehydrated sample.

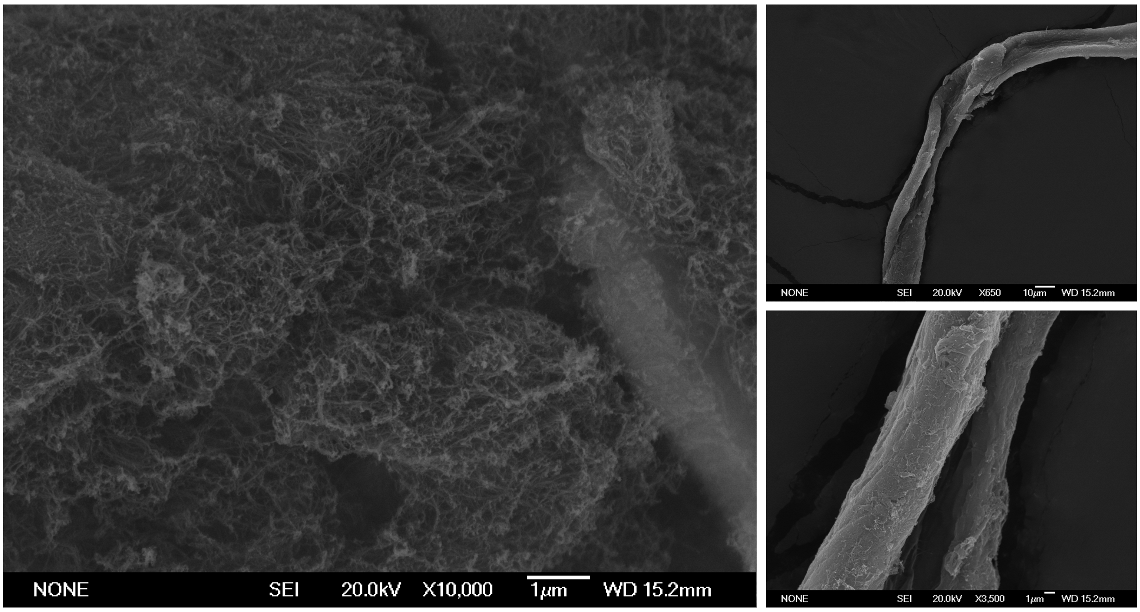

Figure S28. SEM images of **QT:C$_{60}$MA-TH** coassemblies, dehydrated sample.

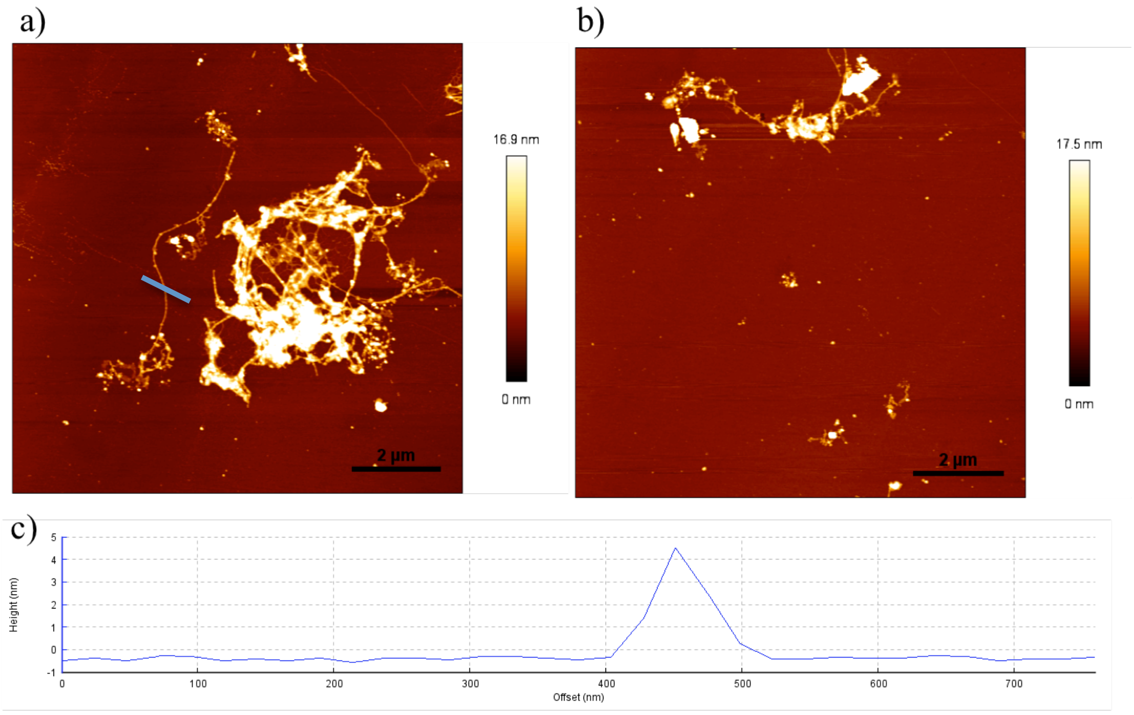

Figure S29. AFM images of **QT:PBI** coassemblies from previously equilibrated solutions of **QT** in citric acid/sodium citrate buffer solution under thermodynamic conditions and **PBI** in MiliQ water (a,b). Height profile of the selected region (blue line) in AFM image a (c).

Table S3. Maximum values of the transients $(\phi\Sigma\mu)_{max}$ for the n/p- materials and the building blocks separately.

n/p- materials	$\phi\Sigma\mu$ ($cm^2\ V^{-1}\ s^{-1}$)	Controls and building blocks	$\phi\Sigma\mu$ ($cm^2\ V^{-1}\ s^{-1}$)
QT:PBI-PBS	1.4×10^{-4}	**QT-PBS**	3.8×10^{-5}
QT:C$_{60}$MA-PBS	3.3×10^{-5}	**QT-TH**	6.3×10^{-5}
QT:PBI-TH	3.2×10^{-3}	**PBI** (from water solution)	1.4×10^{-5}
QT:C$_{60}$MA -TH	1.5×10^{-3}	**C$_{60}$MA** (from water solution)	1.2×10^{-5}
QT:PBI-ME	2.0×10^{-4}	**QT:PBI** in Methanol	1.2×10^{-4}
QT:C$_{60}$MA -ME	3.4×10^{-4}	**QT:C$_{60}$** in Methanol	2.9×10^{-5}

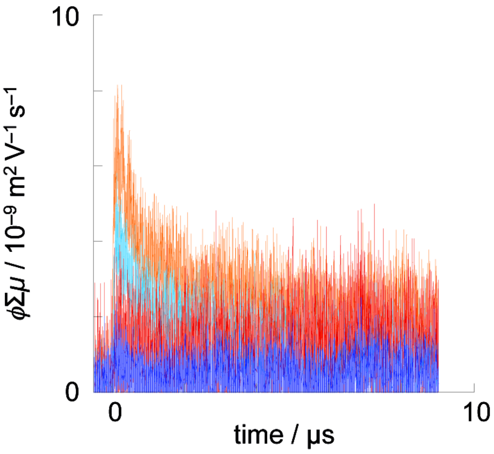

Figure S30. Kinetic traces of conductivity transients observed for films of **QT-TH** (orange), **QT-PBS** (turquoise), **PBI** from water solution (red), and **C$_{60}$MA** from water solution (blue) upon excitation of 355 nm laser pulses at (purple) 9.1×10^{15} photons cm^{-2}.

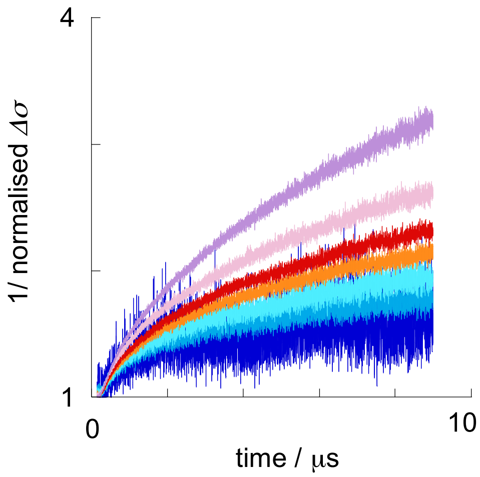

Figure S31. Comparative kinetic traces of conductivity transients observed for a film of **QT:PBI-TH** upon excitation of 355 nm laser pulses at 0.15 (blue), 0.91 (turquoise), 1.8 (sky blue), 4.6 (orange), 6.4 (red), 9.1 (pink), and 18 (purple) × 10^{15} photons cm^{-2}.

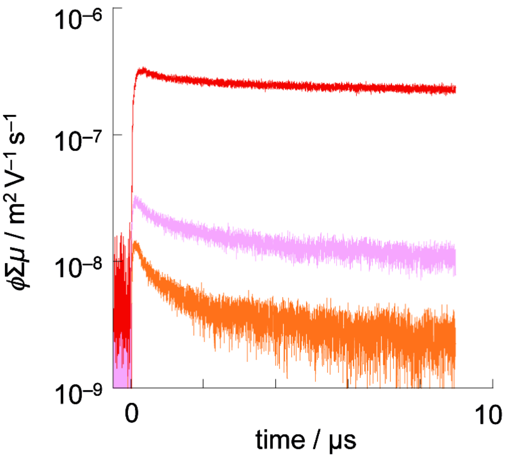

Figure S32. Kinetic traces of conductivity transients observed for a film of **QT-PBI** aggregates upon exposure to 355 nm pulses at 0.15 (**QT:PBI-TH**, red), 0.91 (**QT:PBI-ME**, pink), and 4.5 (**QT:PBI in PBS**, orange) × 10^{15} photons cm^{-2}.

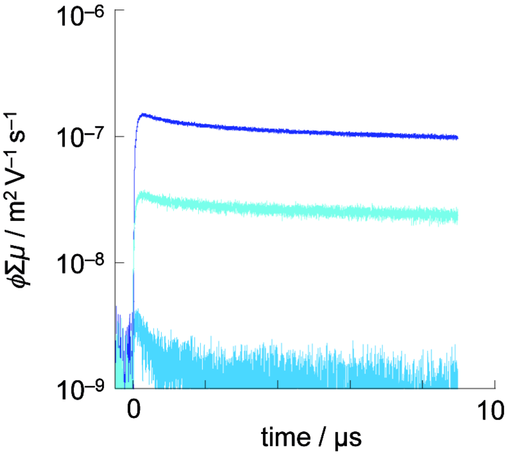

Figure S33. Kinetic traces of conductivity transients observed for **QT-C$_{60}$MA** coassemblies upon exposure to 355 nm pulses at 9.1 × 10^{14} (**QT:C$_{60}$MA-TH**, blue and **QT:C$_{60}$-ME**, skyblue) and 9.1 × 10^{15} (**QT:C$_{60}$MA-PBS**, turquoise) photons cm^{-2}.

7. References

(1) J. Kagan, S. K. Arora and A. Ustunol, *J. Org. Chem.*, **1983**, *48*, 4076

(2) (a) F. Diederich, C. Thilgen, *Science*, **1996**, *271*, 317-324. (b) Y. Ishida, H. Ito, D. Mori, K. Saigo, *Tetrahedron Lett.*, **2005**, *46*, 109-112. (c) Y. Nakamura, M. Suzuki, Y. Imai, J. Nishimura, *Org. Lett.*, **2004**, *6*, 2797-2799.